MICROCOPY RESOLUTION TEST CHART

NATIONAL BUREAU OF STANDARDS-1963-A

SEMICONDUCTOR ELECTRODES. 51.

EFFICIENT ELECTROLUMINESCENCE AT

ZnS ELECTRODE IN AQUEOUS ELECTROLYTES.

by

Fu-Ren F. Fan, Patrick Leempoel and Allen J. Bard

For Publication in the

Journal of the Electrochemical Society

The University of Texas at Austin
Department of Chemistry
Austin, Texas 78712

April 1, 1983

DTIC
ELECTE
APR 2 3 1983
E

83 04 28 130

REPORT DOCUMENTATION PAGE		READ INSTRUCTIONS BEFORE COMPLETING FORM
1. REPORT NUMBER	2. GOVT ACCESSION NO. AD.A127454	3. RECIPIENT'S CATALOG NUMBER
4. TITLE (and Subtitle) SEMICONDUCTOR ELECTRODES. 51. EFFICIENT ELECTRO-LUMINESCENCE AT ZnS ELECTRODE IN AQUEOUS ELECTRO-LYTES.		5. TYPE OF REPORT & PERIOD COVERED 1 Sept. 1982-31 Aug. 1983
		6. PERFORMING ORG. REPORT NUMBER 30
7. AUTHOR(s) Fu-Ren Fan, Patrick Leempoel and Allen J. Bard		8. CONTRACT OR GRANT NUMBER(s) N00014-78-C-0592
9. PERFORMING ORGANIZATION NAME AND ADDRESS Department of Chemistry University of Texas at Austin Austin, TX 78712		10. PROGRAM ELEMENT, PROJECT, TASK AREA & WORK UNIT NUMBERS
11. CONTROLLING OFFICE NAME AND ADDRESS Office of Naval Research 800 N. Quincy Arlington, VA 22217		12. REPORT DATE APRIL 1, 1983
		13. NUMBER OF PAGES 47
14. MONITORING AGENCY NAME & ADDRESS(if different from Controlling Office)		15. SECURITY CLASS. (of this report) Unclassified
		15a. DECLASSIFICATION/DOWNGRADING SCHEDULE

16. DISTRIBUTION STATEMENT (of this Report)

This document has been approved for public release and sale;

its distribution is unlimited.

17. DISTRIBUTION STATEMENT (of the abstract entered in Block 20, if different from Report)

19. KEY WORDS (Continue on reverse side if necessary and identify by block number)

electroluminescence, luminescence, display, semiconductor

20. ABSTRACT (Continue on reverse side if necessary and identify by block number)

Electroluminescence (EL) on ZnS was studied in aqueous solutions containing various redox species. For species able to generate strongly oxidizing intermediates, such as peroxydisulfate or hydrogen peroxide, bright blue luminescence was observed during cathodic polarization at potentials near to or negative of flat-band potential (V_{fb}) of ZnS. For solutions containing supporting electrolyte alone at various pH's, no emission was detectable even at potentials 7 volts negative of V_{fb}. This suggests that minority-carrier (hole) injection is ⟶

DD FORM 1473 EDITION OF 1 NOV 68 IS OBSOLETE
1 JAN 73
S/N 0102-014-6601 |

responsible ofr the initiation of EL. The peak energy of the EL spectrum was much smaller (by 1 eV) than the bandgap of ZnS, suggesting that the radiative recombination is through intermediate luminescent centers. Under steady state conditions, the EL intensity was proportional to the square of the current, suggesting that EL intensity is dominated by the recombination of electron-hole pairs at luminescent centers. In the early part of a potential pulse (especially the first pulse), the growth behavior of EL intensity was strongly affected by the electron trapping of the empty upper luminescent states. The location of theEL spectra depended on the current density and the EL intensity; with increasing EL intensity, a significant blue shift of the emission peak was observed. These results suggest that the overall radiative recombination rate might be limited by electron transfer (through tunneling mechanism) from the occupied upper luminescent states to the empty lower luminescent states. An EL efficiency of 0.2% can be achieved by operating at a current density of 25mA/cm^2.

Accession For		
NTIS GRA&I	☒	
DTIC TAB	☐	
Unannounced	☐	
Justification		
By		
Distribution/		
Availability Codes		
Dist	Avail and/or Special	
A		

DTIC COPY INSPECTED 2

SEMICONDUCTOR ELECTRODES. 51.

EFFICIENT ELECTROLUMINESCENCE AT

ZnS ELECTRODE IN AQUEOUS ELECTROLYTES.

Fu-Ren F. Fan,[*] Patrick Leempoel and Allen J. Bard[*]

Department of Chemistry

The University of Texas at Austin

Austin, Texas 78712

Abstract

Electroluminescence (EL) on ZnS was studied in aqueous solutions containing various redox species. For species able to generate strongly oxidizing intermediates, such as peroxydisulfate or hydrogen peroxide, bright blue luminescence was observed during cathodic polarization at potentials near to or negative of flat-band potential (V_{fb}) of ZnS. For solutions containing supporting electrolyte alone at various pH's, no emission was detectable even at potentials 7 volts negative of V_{fb}. This suggests that minority-carrier (hole) injection is responsible for the initiation of EL. The peak energy of the EL spectrum was much smaller (by 1 eV) than the bandgap of ZnS, suggesting that the radiative recombination is through intermediate luminescent centers. Under steady state conditions, the EL intensity was proportional to the square of the current, suggesting that EL intensity is dominated by the recombination of electron-hole pairs at luminescent centers. In the early part of a potential pulse (especially the first pulse), the growth behavior of EL intensity was strongly affected by the electron trapping of the empty upper luminescent states. The location of the EL spectra depended on the current density and EL intensity; with increasing EL intensity, a significant blue shift of the emission peak was observed. These results suggest that the overall radiative recombination rate might be limited by electron transfer (through a tunneling mechanism) from the occupied upper luminescent states to the empty lower luminsescent states. An EL efficiency of 0.2% can be achieved by operating at a current density of 25 mA/cm^2.

(End of Abstract)

Introduction

The study of interfacial charge-transfer processes at semiconductor electrodes is under active investigation(1-5). Luminescence techniques have been employed successfully as probes to study surface recombination and excited-state processes(6-9). Recently Ellis and co-workers(6) have carried out extensive studies on the electroluminescence and photoluminescence of cadmium chalcogenides, for example CdS and CdSe, and, by comparison with photogenerated charge transfer obtained information about the reaction processes at these electrodes. The efficiency of the room-temperature emission of these materials in the visible spectral region is quite low, as is that of most other semiconductors (e.g. quantum yields $< 10^{-3}$).

Wide bandgap II-VI compounds are potentially useful electrode materials for visible electroluminescence in solution; the zinc chalcogenides are especially good candidates for such applications. Indeed, low voltage solid-state devices which produce electroluminescence have been described; however, it is difficult to produce a good pn junction necessary for efficient charge injection due to self-compensation by native defects. Less complex Schottky junctions have been attempted with some degree of success(10-12). There have been few reports of solution studies of electroluminescence of ZnS (13,14). In an early letter (14) emission was reported for a ZnS electrode immersed in fuming sulfuric acid; this was attributed to the formation of an inversion layer at ZnS surface. More recently a brief report by Tyagai et al (13) described the blue emission of a ZnS cathode in H_2O_2, which was attributed to hole injection from the reduction intermediate, ·OH, into the valence band of ZnS. However, details of the process, the mechanism of emission and the dependence of the spectral distribution on a variety of electrochemical parameters were not explored.

We thought it of interest to examine the electroluminescence of ZnS as a probe of the energetics at the ZnS/electrolyte interface and for possible application to display devices.

In this paper we examine the electrochemical and electroluminescent properties of single-crystal, n-type ZnS electrodes with various redox couples. We demonstrate that the electroluminescence (EL) is initiated by hole injection from solution redox couples and under steady state conditions the EL intensity is dominated by the recombination of electron-hole pairs at luminescent centers. Neither electron transfer to the upper states nor hole transfer to the lower state controls the rate of emission in the condition studied. The effect of trapping on the growth of EL and the factors affecting the intensity and spectral distribution of the EL will be discussed. The EL efficiency at room temperature is among one of the highest in the photoelectrochemical-type luminescent cells or low voltage solid-state electroluminescence devices (22). An EL efficiency of 0.2% can be achieved by operating at a current density of 25mA/cm^2.

Experimental Section:

Materials

Al-doped ZnS single crystals were generously donated by Dr. J. O. McCaldin or were grown by iodine chemical vapor transport(15). These crystals usually had high resistivities ($>10^{10}$ohm-cm). The crystals were heated in a molten 90% Zn - 10% Al mixture at 900°C for 10-24 hours. This treatment reduced the resistivity of some crystals to 20 to 10^4 ohm-cm. The crystals with low resistivity were used in the EL experiments. They were cut into slices along the (111) plane and were subsequently polished by carborundum (1 μm grit size) and alumina (0.5 μm particle size). Ohmic contact was made according to the method given by Kaufman and Dowber (16). The crystals were mounted as electrodes as described previously (17).

Before a series of experiments, the electrode was etched in a potassium dichromate-H_2SO_4 cleaning solution at 70^oC for 5 minutes. Reagent grade chemicals were used without further purification. All solutions were prepared from triply distilled water and were deoxygenated, if not otherwise mentioned, for at least 30 minutes with purified nitrogen before each experiment. These experiments were carried out with the solution under a nitrogen atmosphere.

Electrochemical Measurements

All electrochemical measurements were performed with the same electrochemical cells, apparatus and procedures as reported previosly (17). The impedance measurements were carried out with an aqueous solution containing 1.0 M $NaClO_4$. The pH of the solution was adjusted with $HClO_4$ or concentrated NaOH (10 M). The apparatus and procedures for impedance measurements were based on those reported previously (18). Two a.c. frequencies (100 and 300 Hz) were employed and no significant dispersion was found.

Electroluminescence Measurements

The EL spectra were mainly obtained with a PAR Model 1215 OMA2 optical multichannel analyzer including a Silicon Intensifier Target vidicon detector with a vacuum UV scintillator to enhance the UV response. This detection system has an essentially flat response in the wavelength range of the ZnS EL spectrum, 350-550 nm. To obtain the EL spectra, the electrode was pulsed between 0.0 V vs. SCE and a given negative potential. The EL signal was detected by synchronizing the OMA detection system with the potential pulses applied to the electrode. Another detection system was constructed based on an Oriel monochromator equipped with gratings blazed at 500 or 1000 nm. The monochromator was interfaced to a highly red-sensitive photomultiplier tube (PMT) (Hamamatsu R928). Signals from the PMT were

amplified by a lock-in amplifier and displayed on a Houston Model 2000 X-Y recorder. In the transient experiments, the EL signal was detected by a PMT with attached neutral density filters and a 460 nm band-pass filter. Signals from the PMT were amplified by a current-to-voltage converter and displayed together with the chronoamperometric curves on a Nicolet Model 1090A digital oscilloscope and then recorded on a Houston Model 2000 X-Y recorder.

The integrated EL efficiency, $\bar{\phi}_{EL}$, was determined by an integrating sphere photometric detection system as described by Itaya and Bard (19) and by Bezman and Faulkner (20).

The total photometric appartus consisted of an integrating sphere and an EG & G radiometer attached to the viewing port of the sphere. The sensitivity, S, of the intergrating sphere was calibrated with a He-Ne laser or by a light beam (10 nm band-width) obtained from a 450 W Xe-lamp and an interference band-pass filter at 460 nm. The calibration factor, C, of the EG & G radiometer was obtained by a standard actinometric procedure with a 0.1 M ferrioxalate actinometer. The sample cell for EL experiments was inserted into the sphere and was held in position by a standard taper joint attached to the sphere. The electrode was pulsed and the total charge passed was measured with a digital coulometer. The total photon energy emitted was measured by the integrating sphere photometric apparatus. The integrated number of photons can be calculated based on Eq. (1) given in Ref. 19 or approximately,

the total number of photons (einsteins) $\cong$

S x C x total photon energy (joules) measured/F x photon energy at λ_{max} (1)

in which F is Faraday's constant and λ_{max} is the wavelength at the peak of EL

spectrum. In this equation, the average energy per photon is taken as the photon energy at λ_{max}. This is only an approximation since the EL spectra are not narrow enough to be treated as line spectra. However, they are quite symmetric and the half-width is narrow as compared with the photon energy at λ_{max}.

Results:

Electrochemical Behavior

Flat-band Potential (V_{fb}).--Studies of the capacitance of n-ZnS electrodes were conducted in deaerated aqueous solutions containing 1 M NaClO$_4$ at different pH's. As shown in Fig. 1, a Schottky depletion layer was formed at the surface of ZnS, as indicated by the linear dependence of the reciprocal of the square of the capacitance on the potential (Mott-Schottky plot). V_{fb} of this ZnS electrode was -1.61 V vs. SCE at pH 1.95 and shifted about 55 mV negatively per pH unit increment. The uncompensated ionized charge density, found from the slope of the Mott-Schottky plots and the dielectric constant ($\varepsilon = 8.3$), (21) was 9.1 x 10^{17} cm^{-3}.

Voltammetric Behavior

Cyclic voltammetric studies on n-ZnS were conducted in deaerated 1 M NaCl solution at different pH's. As shown in Fig. 2, in the absence of peroxydisulfate at pH 11.4, no appreciable cathodic current was observed at potentials positive of -2.0 V vs. SCE (curve a). The introduction of 20 mM K$_2$S$_2$O$_8$ into the solution caused an increase in the cathodic current for potentials negative of -1.8 V vs. SCE (cur b). This enhanced cathodic current is apparently due to the reduction of S$_2$O$_8{}^{2-}$ at the ZnS electrode. When the pH of the solution used in b was decreased to 2.2, a diffusion-controlled reduction wave with a peak current, i_p, proportional to the square root of scan rate and a peak potential, E_p, at about -1.85 V vs.

SCE appeared (curve d). This wave can mainly be attributed to proton reduction, because the peak height increases with the proton concentration (compare curve e with curve d) and the peak position was essentially the same as that corresponding to proton reduction in a solution not containing $S_2O_8^{2-}$ (see curve c). However the different i_p-values in curves d and c suggest partial contribution by the reduction of peroxydisulfate species. The reduction of $S_2O_8^{2-}$ does not appear to be strongly pH dependent over the pH range studied. Note that the peak position for $S_2O_8^{2-}$ reduction of graphite electrodes is essentially pH independent (see Fig. 3).

Interfacial Energy Scheme

The interfacial energy scheme at the (ZnS/electrolyte) interface at pH 1 is summarized in Fig. 4. The location of the band edges of ZnS with respect to SCE were calculated based on the procedures reported previously [18] and the following quantities: the resistivity of the sample, $\rho \cong 20$ ohm-cm; the effective mass of electron, $m_e^* = 0.34 \, m_0$ [21] (m_0 is the mass of free electron); the electron mobility, $\mu_e = 160 \, cm^2/V.sec$ [22]; the bandgap, $E_g = 3.66$ eV [21,22] and the flat-band potential at pH 1, $V_{fb} = -1.54$ V vs. SCE. The conduction band edge, E_c, was found to be -1.74 V vs. SCE. This put the valence band edge, E_v, at a potential of 1.92 V vs. SCE. The normal potentials of the (OH⁻/OH) and (SO_4^{2-}/SO_4^{-}) couples have been estimated to be 2.7 V and 3.2 V vs. SCE, respectively [23].

Electroluminescence (EL).

Studies of EL from n-ZnS electrodes were conducted in deaerated aqueous solutions containing various redox couples given in Fig. 4 or in oxygen-saturated solution containing no redox couples other than supporting electrolyte, 1 M $NaClO_4$. In the presence of peroxydisulfate or hydrogen peroxide a bright blue emission was observed starting at potentials negative of V_{fb} that was readily observable under day light conditions (Fig. 5). No detectable EL was observed in solution containing only supporting

electrolyte even at an applied potential of -10 V vs. SCE. In Ce(IV) solution, the blue emission was found at potentials far negative of V_{fs}, such as -5 V vs. SCE. EL with peroxydisulfate was studied most extensively, and details of the results in solutions containing 0.2 to 1 M $S_2O_8^{2-}$ at different pH's are given below.

Steady-State Current and EL-Potential Properties.--As shown in Fig. 6a, the current, i, increases exponentially with potential, and some cathodic current flows when the potential is positive of V_{fb}. This exponential dependence is consistent with the capacitance measurements which indicate the formation of a Schottky depletion layer at the surface of ZnS. When the potential is well negative of V_{fb}, the i-ΔV (where $\Delta V = V - V_{fb}$) characteristic obeys a power-law relationship over a wide range of applied potential of the form $i \propto \Delta V^n$ with n equal to 2. This suggests that the current in this potential range is dominated by double injection (24). A current doubling effect is expected with this system based on the interfacial energy scheme shown in Fig. 4.

Different from the i-ΔV behavior, significant EL intensity is only detected at potentials near to or negative of V_{fb} (see Fig. 6b), where double injection takes place. Moreover, the EL intensity rises more steeply, as compared with the current, with increasing negative potential. As shown in Fig. 7 the EL intensity, I, varies according to a relationship of the form $I \propto i^n$, with n equal to 2 over the current range studied.

Spectral Distribution--EL spectra were obtained by repetitively pulsing the electrode between 0.0 V and a potential negative of V_{fb}. The bright blue emission could be seen easily with the naked eye even under ordinary room light conditions. The EL spectra were obtained by synchronizing the OMA detection system with the potential pulses applied to the electrode.

Since the intensity and the spectral distribution of the EL vary with time during the first several potential pulses and reach a steady-state condition only after some period of cycling, the EL spectra shown were recorded under steady-state potential pulsing conditions, if not otherwise mentioned. The EL growth behavior is described in the following sections.

The EL spectra, shown in Fig. 8, are characterized by a single broad band with maximum EL intensity at about 460 nm. The exact peak position, λ_{max}, of the EL spectrum depends on several parameters which will be discussed in the following sections. Because the sensitivity of the OMA detection system was low at wavelengths beyond 700 nm, a highly red-sensitive photomultiplier tube (Hamamatsu R928) was used to check the EL spectrum in this region. No other bands were observed out to 1000 nm.

Effects of Potential on EL Intensity and Spectral Distribution.--As shown in Fig. 8, significant changes in the intensity and shifts in spectral distribution of the EL were found with small changes of the negative potential limit. More negative step potentials increased the EL intensity and produced a blue shift in the EL spectrum (by about 35 nm in λ_{max} with a potential change of -1.95 to -2.25 V vs. SCE). The EL spectrum also was broadened with decreasing negative limits (half-width of 92 nm at -1.95 V vs. 84 nm at -2.25 V vs. SCE). Note that the EL spectrum with the higher emission intensity had a sharper high-energy edge than that with low emission intensity. This is shown more clearly in Fig. 9 by normalizing curve e in Fig. 7 to the same peak height as curve a and then translating this normalized curve by 35 nm to shorter wavelengths to match the peak positions of the two curves.

Development of Electroluminescence and Current during Sequential Potential Pulses.--The growth and decay of the EL intensity and current during a sequence of potential pusles between 0 and -2.75 V vs. SCE is shown in Fig.

10. In the first pulse, the current (the lower curve) reaches a peak value within 5 μsec, which is very close to the rise time of the potential step generated from the potentiostat. After reaching the maximum, the current decays exponentially to a steady state value. In the subsequent pulses, this current overshoot disappeares gradually and the current more rapidly (∿ 20 μsec) attains the steady-state value. In the reverse (positive) potential step, the current decays to zero within 20 μsec and occasionally shows an oscillation. The increase of EL intensity was slower than the corresponding rate of current increase and no significant decay occurred during the cathodic step, if the pulse width was short ($\leq$5 msec.) (Fig. 10). The EL intensity increased with sequential potential pulses and reaches a steady-state value after about 10 pulses, if the cathodic step potential was negative of -2.5 V vs. SCE. The decay time of EL ($\leq$ 20 μsec) was much shorter than its rise time. The rise time depended on the history of pulsing and the step potential. Extensive potential pulsing and/or a large amplitude potential step decreased the rise time of EL. A rise time of 200 μsec can be achieved after extensive pulsing of the ZnS electrode between 0 and -3.5 V vs. SCE. There was always a dead zone at the beginning of the first potential pulse of a sequence where significant current was observed without generation of a significant amount of EL.

Accompanying the growth of the EL intensity during a sequence of pulses, a blue-shift of the EL spectrum was observed. As shown in Fig. 11, the integrated EL intensity during a single pulse increased with pulse number. This is consistent with the result shown in Fig. 10. The integrated EL intensity in the 26th pulse was about 100 times higher than that of the first pulse. Moreover, a pronounced blue shift of about 20 nm in λ_{max} was observed on the EL spectrum of the 26th pulse compared to that

of the first.

Effects of pH on EL Intensity and Spectral Distribution--Studies of pH

effects on the EL were conducted in deaerated solutions containing 0.2 M

$(NH_4)_2S_2O_8$ and 1 M $NaClO_4$. The pH of the solution was adjusted with 10M

NaOH and $HClO_4$.   The peak intensity of the EL was a function of pH (Fig.

12). When the potential of the ZnS electrode was pulsed between 0 and -3 V

vs. SCE with a 5 msec. pulse width, the EL intensity reached a maximum

value at pH 7-9 and decreased gradually at lower pH and more steeply at

higher pH. An increase in pH from 8.0 to 10.1 caused a large decrease in the

EL intensity and a red shift of 35 nm in the EL spectrum. Similarly, a

decrease of pH from 8.0 to 1.2 decreased the EL intensity and caused a

red-shift ($\sim$18 nm) of the EL spectrum (Fig. 13).

Electroluminescence in the First Potential Pulse--The growth of EL during

the first pulse was usually very different from that observed under

steady-state pulse conditions. The effect of the negative potential limit

is shown in Fig. 14. At smaller negative potentials (e.g. positive of -2 V

vs. SCE), the EL intensity was very low and increased linearly with time

(see curve 14a).   As the limit was made more negative, the EL intensity

increased linearly with time at the very beginning and exponentially

approached a saturation value at longer times (see curve 14c), indicating a

faster growing-in of EL as compared with that at less negative potentials.

A faster rate in EL growth could also be achieved at less negative

potentials, if the electrode was pre-biased to a potential where no EL was

generated but a significant current was observed (for example, a pre-bias at

any potential between -1.4 and -1.8 V vs. SCE at pH 8.4).

The effect of pre-bias on the growth behavior of EL at -2.25 V vs. SCE

is shown in Fig. 15. Without pre-bias, the EL intensity was low and grew

very slowly (see curve b).   The corresponding chronoamperometric curve

(curve d) showed a significant current overshoot and sharp decay to a steady-state value. Pre-bias of the electrode for 30 sec. at -1.72 V vs. SCE, where no EL but a significant transient current was detected, not only enhanced the EL intensity but also accelerated the growth of EL (see curve a). The current overshoot in curve d disappeared and the current reaches the steady-state value within a few tens of μsec (see curve c).

Efficiency and Stability of ZnS Electrode--The EL efficiency was determined in a pulse experiment with a step potential to -2.5 V vs. SCE where a steady-state current density of 25 mA/cm^2 was obtained. An integrated EL efficiency, ϕ_{EL}, was calculated based on Eq. (2)

$$\bar{\phi}_{EL} = \frac{\text{Total light emitted} \times F}{\text{Total charge passed through the electrode}} \qquad (2)$$

in which F is Faraday's constant, the light emitted was in einsteins and the charge in coulombs. The total light energy, in joules, was converted to einsteins at 460 nm. The broad (fwhm of $\sim$80 nm) but quite symmetric feature of the EL spectrum makes this only an approximation. The EL efficiency at a current density of 25mA/cm^2 ranged from 0.2 to 0.35%, depending on the particular electrode. Since the EL intensity depends in a nonlinear way on the current density, as illustrated in Fig. 7, so does ϕ_{El}. To investigate the stability of the ZnS electrodes in aqueous solution containing peroxydisulfate, we performed a long-term pulse experiment. The electrode was immersed in a solution containing 0.2 M $(NH_4)_2S_2O_8$ and 1 M $(NH_4)_2HPO_4$ (pH $\sim$ 8) and was pulsed between 0 and -2.5 V vs. SCE with a pulse width of 5 msec. The EL intensity was monitored occasionally with a radiometer. Since peroxydisulfate is reduced irreversibly on the ZnS electrode and is not regenerated at the counter electrode, an additional amount of peroxydisulfate was introduced daily into the solution. The pH of

the solution was kept at ~8. The EL intensity showed some short-term fluctuation but the electrode glowed continuously for at least 11 days, after which time the experiment was terminated. The surface of the electrode after this test was darker colored than originally but the weight loss was < 1%. At present we are uncertain as to the origin of the apparent change of the electrode surface color. The darkening of the electrode surface did not decrease the EL intensity and the surface film was difficult to remove by etching with dichromate cleaning solution.

Discussion

Interfacial Energetics and Mechanism of Electroluminescence.

The fact that significant EL intensity near V_{fb} occurs only in solutions containing redox couples, such as H_2O_2 and $S_2O_8^{2-}$, whose reduction produces intermediates that are sufficiently oxidizing to inject holes into the valence band of n-ZnS (see Fig. 4), supports the minority-carrier injection mechanism of electroluminescence (6-8,13). The lack of EL in supporting electrolyte alone and the observation of little EL in solutions containing weakly oxidizing species, such as $Fe(CN)_6^{3-}$, even at a potential far negative of V_{fb} (for example -8.0 V vs. SCE), rules out the possibility that the energetic holes required for EL are generated by high electric field processes inside the semiconductor, e.g. field-assisted electron tunneling from valence band to conduction band. In solutions containing redox couples with potentials located within the band gap but close to the valence band edge of n-ZnS, such as Ce(IV)/Ce(III) and Tl(II)/Tl(I), significant EL was observed only when the n-ZnS electrode was biased at a potential at least 1 V negative of V_{fb}. The requirement of this overpotential is understandable simply based on the energetics for

interfacial hole transfer. Both Ce(IV) and Tl(II) are energetically insufficient to inject holes into the valence band of n-ZnS. However, efficient hole injection can occur, if a significant net change in the potential drop across the double layer is allowed or a strong negative bias is applied to the electrode so that electron tunneling from the valence band to the solution species can take place. This seems the case for Ce(IV) and Tl(II).

The mechanism proposed for the electroluminescence in $S_2O_8^{2-}$ or H_2O_2 is shown in Scheme I. This scheme has long been applied to explain the edge emission from GaP, CdSe, etc.

$$A_2 + e^- \rightarrow A\cdot + A^- \quad (3)$$

$$A\cdot \rightarrow A^- + h^+ \quad (4)$$

Scheme I
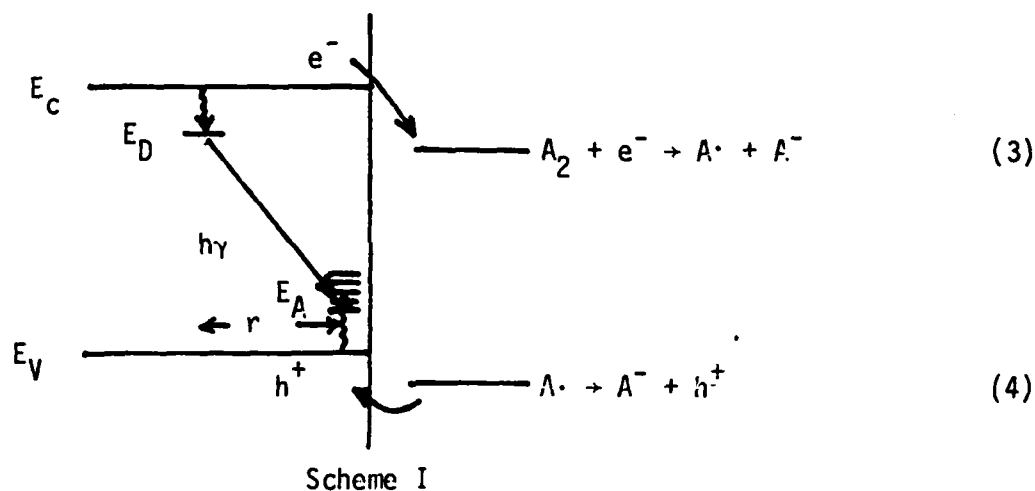
The first stage (Eq. 3) involves the reduction of $S_2O_8^{2-}$ or H_2O_2 by conduction-band electrons of the n-ZnS electrode. This produces SO_4^- or OH; these are sufficiently oxidizing to capture electrons from the valence band in the second stage (Eq. 4). The radiative recombination of these injected holes with conduction-band electrons does not produce edge emission (corresponding to E_g) in the present experiment. The peak energy (2.74 eV) of the EL spectrum is substantially smaller than the bandgap (3.66 eV) of ZnS. This subband-gap emission can only be explained based on radiative recombination through intermediate levels, such as the donor impurity level

E_D and/or acceptor impurity level E_A.

The interfacial energetics can also be changed by varying the pH of the solution. Capacitance measurements clearly show the strong pH dependence of V_{fb} of n-ZnS electrodes. Increasing the pH shifts V_{fb} towards more negative values. This favors hole injection (Eq.(4) in Scheme I) but makes electron transfer from the conduction band of n-ZnS to solution species (the first step or Eq. (3) in Scheme I) less favorable. Thus at a given potential, the current density and the corresponding EL intensity decrease with an increase in pH. This is consistent with the results shown in Fig. 12 when the pH is beyond 8. The decrease of EL intensity with a decrease in pH at pH < 7 does not fit this argument. The decrease of EL intensity in this pH range might be caused by at least two factors. The first involves the competition between the reduction of proton and $S_2O_8^{2-}$ on the ZnS electrode. This is illustrated in Fig. 2. Proton reduction which produces no EL, would decrease the contribution of the reduction of $S_2O_8^{2-}$ to the total current density and thus reduces the EL intensity. The second factor pertains to the instability of ZnS in acidic solution. Significant weight loss ($\sim 5\%$) was observed after a ZnS crystal was immersed in an air-saturated solution containing 1 M $(NH_4)_2S_2O_8$ at pH 1 for two months.

Spectral Distribution and Intensity of Electroluminescence

That EL spectra are more asymmetric at high emission intensity than at low intensity as shown in Fig. 9 might be partially due to the effect of self-absorption. If holes can be transferred from some distance into the ZnS, the photons emitted there (especially those with shorter wavelength) could be recaptured to promote photo-induced electron transfer from traps. Experiments showing a photo-enhanced cathodic current and photo-quenching of EL, which will be discussed in a separate paper, support this argument. The sharper rise in intensity in the high-energy edge is expected from the

reabsorption of the luminescence by the transition between the band tail (caused by heavily doping) and filled intermediate levels. These results suggest that EL from ZnS is produced in a region extending from the seminconductor/solution interface into a certain depth of the semiconductor. However, due to the much lower ($\sim$16 times) hole mobility compared with the electron mobility, the emission zone could be quite thin.

One of the interesting features of the EL spectrum on the ZnS electrode is the blue shift of λ_{max} with increasing excitation rate (current density) and thus EL intensity. Several experiments have been conducted to illustrate this phenomenon. These include (1) the effect of cathodic step potential (see Fig. 8), (2) the time dependence of EL spectrum (see Fig. 11) and (3) the pH effect (see Fig. 13). Such peak shifts might be attributed to a kinetic effect involving the rate of filling of holes in a band of acceptor levels involved in the radiative process. Thus at low currents only the upper acceptor levels would be populated, resulting in lower energy transition, while at high currents, lower acceptor levels would be involved and a higher energy transition would be observed. If this mechanism applies, one would expect the low-energy edge of the EL spectrum to reproduce approximately the shape of the acceptor band at the low-energy tail. This seems consistent with the experiment, if the impurity band has an exponential distribution of states at the low-energy edge. However, the high-energy edge of the EL spectrum should be a rather abrupt cutoff before the impurity band is completely filled. The experiment does not show this behavior especially at low current densities (low EL intensities).

One of the accepted models to explain this phenomenon and most of our results on luminescence (including photoluminescence and photoquenching of EL which are not reported here) at ZnS involves tunneling between spatially separated upper (or donor) and lower (or acceptor) states (see Scheme 1).

This concept was proposed about two decades ago by Williams and coworkers (25) to explain luminescence from Cu-doped and Cu In-doped ZnS. Similar recombination processes by electron tunneling have been identified for donor-acceptor pairs in many semiconductors (26-28) and in alkali halides (29).

The energy of the emitted light due to the transition from the donor level to the acceptor level in a donor-acceptor pair separated by a distance, r, is given by (21) Eq.(5), if the phonon coupling is neglected,

$$E(r) = E_g - (E_A + E_D) + e^2/\epsilon_o r, \qquad (5)$$

in which E_g is the band gap, E_A and E_D are the depth of the donor and acceptor, respectively, e is the elementary charge and ϵ_o is the static dielectric constant. The electron tunneling probability between two states can be written (30,31)

$$W(r) = W_o \exp (-2r/a) \qquad (6)$$

where a is the effective radius for overlap of the donor wave functions with the acceptor wave functions and W_o is a parameter independent of r.

Based on the tunneling model, the rate-determining step for the overall radiative recombination process is the electron transfer (through a tunneling mechanism) between the occupied upper states and the empty lower states. With progressive excitation by a potential pulse of large amplitude, electrons are accumulated in the upper luminescent levels and holes in the lower levels. This increases the density of excited luminescent states and thus statistically shortens the average inter-impurity distance. A blue shift of the emission peak (Eq. 5) with

increasing transition probability (Eq. 6) should be observed. However, since the number of possible pairings decreases as r decreases, (25c,26c) the emission intensity must go through a maximum as the separation r is varied. Qualitatively, this model explains the relation between the spectral distribution and the EL intensity quite satisfactorily.

Electroluminescence Intensity-Current Relationship

The intensity (I)-current (i) relationship of the form $I \propto i^2$ suggests that the radiative recombination of electron-hole pairs at the luminescent centers is the rate-determining step of the EL under steady-state conditions. Neither electron transfer to the upper states nor hole transfer to the lower state controls the rate of emission. This is consistent with the tunneling model discussed above.

At steady-state, the electron density of the upper occupied state, n_u, is proportional to $\exp[e(QFLE)/kT]$ and the density of free electrons, n. The QFLE term represents the quasi-Fermi level of electrons, k is the Boltzmann constant and T is the absolute temperature. Assuming that the diffusive component of the current is negligibly small as compared to the migration term, the current density is thus proportional to N. Hence, we have

$$n_u \propto i \tag{7}$$

The hole density of the lower empty state, p_{ℓ}, is proportional to $\exp[e(QFLH)/kT)]$ and the density of free holes, p. The QFLH term is the quasi-Fermi level of holes. p is proportional to the rate of hole injection which contributes one half of the total current. The splitting of QFLH and QFLE from the equilibrium Fermi level arises because electrons accumulate in the donor levels and holes accumulate in the lower acceptor states. Thus, we have

$$p_\ell \propto i \quad (8)$$

Since the emission rate is proportional to the product of n_u and p_ℓ, if the radiative recombination process is the rate-determining step, a square law for the intensity-current relationship, is predicted.

Effect of Trapping on the Growth of Electroluminescence

Several experimental results demonstrate the existence of electron trapping, which strongly affects the EL on ZnS: (1) there is a potential region where no EL intensity is detected but significant current is observed (see Fig. 6). (2) the current overshoots in the first potential pulse; pre-biasing the electrode or pulsing the electrode continuously eliminates this current overshoot (see Figs. 10 and 15); this suggests that the current overshoot at the beginning of the first potential pulse is not controlled by solution double layer; (3) at a low negative step potential, the EL intensity is very low and inceases linearly with time (see Fig. 14). Progressively pulsing the electrode accelerates the growing-in of EL and increases also the EL intensity (see Fig. 10). The increase of cathodic limit potential has the same effect on the growth of EL (see Fig. 14).

A simple rate equation is adequate to illustrate qualitatively these points (see Scheme II). If the upper (donor) states are sufficiently deep that the detrapping of electrons to the conduction band can be neglected, the rate of electron filling of the initially empty upper (donor) states is given by

$$\frac{dn_u}{dt} = A_1 n (n_D - n_u) - A_2 n_u p_\ell - A_3 n_u p_\ell \quad (9)$$

in which n_u is the density of occupied upper (donor) states, n the density of electrons in the conduction band, n_D the total number of upper states (empty and occupied) per unit volume, p_ℓ the density of empty lower (acceptor) states, and A_1 and A_2 are constants describing the rate of generation of n_u, the radiative recombination rate and the non-radiative recombination through n_u and p_ℓ, respectively.

We assume that before most of the upper states are filled, electron trapping by these states is the predominant process for the consumption of electrons injected from the bulk of semiconductor into the emission zone. Thus, in the early part of the pulse, n, p and p_ℓ are small and only slowly-varying variables, i.e.

$$\frac{dn}{dt} \sim 0 \tag{10a}$$

$$\frac{dp}{dt} \sim 0 \tag{10b}$$

$$\frac{dp}{dt} \sim 0 \tag{10c}$$

By integration of Eq. 9 with $n_u = 0$ at $t = 0$ and the assumptions in Eqs. 10a, 10b and 10c,

$$n_u = n_u^\infty [1 - \exp\ (-t/\tau)] \tag{11}$$

in which

$$n_u^\infty = A_1 n n_D / (S_1 n + A_2 p_\ell + A_3 p_\ell) \tag{12}$$

and

$$\tau = 1/(A_1 n + A_2 p_\ell + A_3 p_\ell \tag{13}$$

The EL inten ity is given by

$$I = A_2 n_u p_\ell = A_2 p_\ell n_u^\infty\ [1 - \exp\ (-t/\tau)] \tag{14}$$

This exponential growth of EL was observed at high step potentials and in the time domain away from the beginning of a potential step (Fig. 14).

When $t/\tau \to 0$, Eq. (14) reduces to

$$I = A_2 \beta_{\ell} \, n_u^\infty t/\tau \tag{15}$$

This linear growth behavior of EL is observed at the beginning of any potential step or throughout the whole width of potential pulse, when its amplitude is small (see curve a of Fig. 14).

The conservation of charges gives

$$\frac{dn_u}{dt} + \frac{dn}{dt} - \frac{d}{dt} - \frac{dp_{\ell}}{dt} = i_d \tag{16}$$

with

$$i_d = i_T - (i_{f \cdot e} + i_{f \cdot h}) \tag{17}$$

i_d in these equations should represent the current overshoot in the chronoamperograms in the first potential pulses. Combination of Eqs. (10a), (10b), (10c), (12) and (16) yields

$$i_d = (n_u^\infty/\tau) \, \exp \, (-t/\tau) \tag{18}$$

This current transient is clearly shown in the first potential pulse in Fig. 10. The time constant for the increase of EL is very similar to that for the current decay, as expected from Eqs. (14) and (18).

The actual mechanism is certainly more complicated than that given above and involves radiationless recombinations between n and p, probably via trapping levels. These radiationless processes are what contribute to the modest efficiency of the observed EL. Additional surface quenching

processes by solution species also occur. Such processes are currently under investigation.

Conclusions

Bright blue EL results from the electrochemical reduction of peroxydisulfate at a n-ZnS electrode. This luminescence arises from recombination of an electron with a hole injected by an intermediate (SO_4^-) in the reduction.

Acknowledgment

References:

1.   A. Heller, Acc. Chem. Res., 14, 154, (1981).

2.   A. J. Bard, Science (Washington, D.C.) 207, 139, (1980).

3.   M. S. Wrighton, Acc. Chem. Res., 12, 303 (1979).

4.   A. J. Nozik, Annu. Rev. Phys. Chem., 29, 189 (1978).

5.   H. J. Gersicher, J. Electroanal. Chem. Interf. Electrochem., 58, 263 (1975).

6.   (a) H. H. Strickert, J.-R Tong, A. B. Ellis, J. Amer. Chem. Soc., 104, 581 (1982); (b) B. R. Karas, H. H. Strickert, R. Schreiner, A. B. Ellis; Ibid, 103, 1648 (1981); (c) B. R. Karas, A. B. Ellis, Ibid, 102, 968 (1980); (d) B. R. Karas, A. B. Ellis, Ibid, 101, 236 (1979); (e) H. H. Strickert, J.-R Tong, A. B. Ellis, Ibid, 104, 581 (1982); references therein.

7.   B. Pettinger, H.-R. Schoppel, H. Gerischer, Ber. Bunsenges. Phys. Chem., 80, 849 (1976).

8.   K. H. Beckmann and R. Memming, J. Electrochem. Soc., 116, 368 (1969).

9.   (a) J. D. Luttmer and A. J. Bard, J. Electrochem. Soc., 126, 414 (1979); Ibid, 125, 1424 (1978); (b) R. N. Noufi, P. A. Kohl, S. N. Frank and A. J. Bard, Ibid, 125, 246 (1978).

10.   M. Aven and J. Z. Devine, J. Luminesc., 7, 195 (1973).

11.   M. E. Ozsan and J. Woods, Appl. Phys '_(. .., 25, 489 (1974).

12.   H. Katayama, S. Oda and H. Kukimoto, Appl. Phys. Lett., 27, 697 (1975).

13.   V. A. Tyagai, M. K. Sheinkman, E. L. Shtrum, G. Ya. Kelbasov and N. K. Moiseava, Sov. Phys. Semicond., 14, 112 (1980).

14. L. J. Van Ruyven and F. E. Williams, Phys. Rev. Lett. 16, 889 (1966).

15. R. Nitsche, J. Phys. Chem. Solids, 17, 163 (1960).

16. R. G. Kaufman and P. Dowbor, J. Appl. Phys., 45, 4487, (1974).

17. F.-R. Fan, H. S. White, B. L. Wheeler and A. J. Bard, J. Amer. Chem. Soc., 102, 5412 (1980).

18. F.-R. Fan and A. J. Bard, J. Electrochem. Soc., 128, 945 (1981).

19. K. Itaya and A. J. Bard, J. Phys. Chem. 85, 1358 (1981).

20. R. Bezman and L. R. Faulkner, Anal. Chem., 43, 1749 (1971).

21. J. I. Pankove, "Optical Processes in Semiconductors", Prentice-Hall; (Englewood Cliffs, N. J. 1971) 412.

22. Y. S. Park and B. K. Shin, "Topics in Applied Physics", J. I. Pankove (Ed.), Springer-Verlag, (Berlin, 1977) Vol. 17, p.136.

23. R. J. Memming, J. Electrochem. Soc., 116, 785 (1969).

24. M. A. Lampert and A. Rose, Phys. Rev., 121, 26 (1961).

25. (a) J. S. Prener and F. E. Williams, J. Electrochem. Soc., 103,342 (1956); (b) E. F. Apple and F. E. Williams, Ibid, 106, 224 (1960); (c) F. E. Williams, J. Phys. Chem. Solids, 12, 265 (1960).

26. (a) J. J. Hopfield, D. G. Thomas and M. Gershenzon, Phys. Rev. Lett., 10, 162 (1963); (b) D. G. Thomas, M. Gershenzon and F. A. Trumbore, Phys. Rev., 133, 269 (1964); (c) D. G. Thomas, J. J. Hopfield and W. M. Augustyniak, Phys. Rev., A140, 202 (1965).

27. D. Redfield, J. P. Wittke and J. L. Pankove, Phys. Rev., B2, 1830 (1970).

28. R. A. Street, Adv. Phys., 30, 593 (1981).

29. C. J. Delbecq, Y. Toyozawa and P. H. Yuster, Phys. Rev., B9, 449 (1974).

30. A. Miller and E. Abrahams, E. Phys. Rev., 120, 745 (1960).

31.   F. Mott, _Phil. Mag._, **19**, 835 (1969).

Figure Captions

Fig. 1   Mott-Schottky plots of ZnS electrodes in 1 M $NaClO_4$ at different pH. A. C. frequencies, 100 and 300 Hz. Δ, pH 1.95; $\square$, pH 7; $\bigcirc$, pH 10.

Fig. 2   Cyclic voltammograms on ZnS electrodes. Scan rate; 100 mV/sec in (a) 1.0 M $NaClO_4$, pH 11.4; (b) 1.0 M $NaClO_4$, 20 mM $K_2S_2O_8$, pH 11.4; (c) 1.0 M $NaClO_4$, pH 2.3; (d) 1.0 M $NaClO_4$, 20 mM $K_2S_2O_8$ at pH 2.2; (e) 1.0 M $NaClO_4$, 20 mM $K_2S_2O_8$ at pH 2.0. Solution pH was adjusted with concentrated NaOH (10 M) and $HClO_4$.

Fig. 3   Cyclic voltammograms on graphite electrode. Scan rate, 100 mV/sec in (a) 1.0 M Na ClO_4, pH 11.4; (b) 1.0 M $NaClO_4$, 20 mM $K_2S_2O_8$, pH 11.4; (c) 1.0 M $NaClO_4$, 20 mM $K_2S_2O_8$, pH 2.2.

Fig. 4   Energy scheme at ZnS/Electrolyte interface.

Fig. 5   Photo of EL at ZnS electrode.

Fig. 6   Current-(curve a) and EL intensity-(curve b) vs. potential at ZnS electrodes in 1.0 M $NaClO_4$ and 0.2 M $(NH_4)_2S_2O_8$ at pH 8.4. Scan rate, 20 mV/sec.

Fig. 7   EL intensity vs. current for ZnS electrodes in 1.0 M $NaClO_4$ and 0.2 M $(NH_4)_2S_2O_8$ at pH 8.4.

Fig. 8   Steady state EL spectra at different step potentials on ZnS electrodes in 1.0 M $NaClO_4$ and 0.2 M $(NH_4)_2S_2O_8$ at pH 8.9. The positive limit potential was 0 V vs. SCE. Negative limit potentials; (a) -2.25 V, (b) -2.20 V; (c) -2.15 V; (d) -2.10 V; (e) -2.05 V vs SCE.

Fig. 9   EL spectra from curves a and e in Fig. 8 normalized curve e to the same peak height as curve a and then this normalized curve

translated 35 nm to shorter wavelengths to match the peak positions of these two curves.

Fig. 10   Bottom: Current-time characteristics of ZnS electrodes in 1 M $NaClO_4$ and 0.2 M $(NH_4)_2S_2O_8$ at pH 8.4. The potential was pulsed between 0 and -2.75 V vs. SCE at a frequency of 100 Hz. Top: corresponding EL intensity-time characteristics.

Fig. 11   Development of EL spectra for different potential pulses on ZnS electrodes in 1.0 M $NaClO_4$ and 0.2 M $(NH_4)_2S_2O_8$ at pH 8.9. Curve a: 26th pulse; curve b: 11th pulse; curve d: first pulse; curve c: 5 times expansion of the EL scale in curve d. Potential of the electrode was pulsed between 0 and -2.25 V vs. SCE at a frequency of 100 Hz.

Fig. 12   EL peak intensity vs. pH characteristics of ZnS electrodes in 1 M $NaClO_4$ and 0.2 M $(NH_4)_2S_2O_8$. The electrode was pulsed between 0 and -3 V vs. SCE at a frequency of .100 Hz.

Fig. 13   EL spectra at different pH on ZnS electrodes in 1 M $NaClO_4$ and 0.2 M $(NH_4)_2S_2O_8$. The electrode was pulsed between 0 and -2.25 V vs. SCE at a frequency of 100 Hz. Curve a: pH 8.0; b: pH 7.4; c: pH 5.0; d: pH 2.7; e: pH 1.2; f: pH 10.1.

Fig. 14   Growth behavior of EL of ZnS electrodes during the first pulse. Solution contained 1.0 M $NaClO_4$ and 0.2 M $(NH_4)_2S_2O_8$ at pH 4.0. The cathodic step potential: -2.0 V vs. SCE (curve a); -3.0 V (curve b); -3.5V (curve c).

Fig. 15   Effect of pre-bias on the growth of EL and current for the first potential pulse. Solution and electrode, same as in Fig 14. Curves a (EL) and c (current): electrode was pre-biased at -1.75 V vs. SCE for 30 sec. before step to -2.25 V; curves b (EL) and d (current): without pre-bias.

$$A_2 + e^- \rightarrow A\cdot + A^- \qquad (3)$$

$$A\cdot \rightarrow A^- + h^+ \qquad (4)$$

Scheme I

i_T

E_c n $i_{f,e}$

n_u (n_D) ---- $A_2{}^{2-} + e^{\ominus} \rightarrow A^{2-} + A^{\cdot -}$

p_ℓ

E_v

p $\rightarrow$ ---$A^{\cdot -} \rightarrow A^{2-} + h^{\oplus}$

$i_{f,h}$

Bulk
Semiconductor   Emission zone   solution

Scheme II

Fig.

200 μA

d

e

c

b

a

→cathodic

0   -1.0   -2.0

V vs. SCE

Fin. 2

Fig.

Fig.

(a)

(b)

Fig.
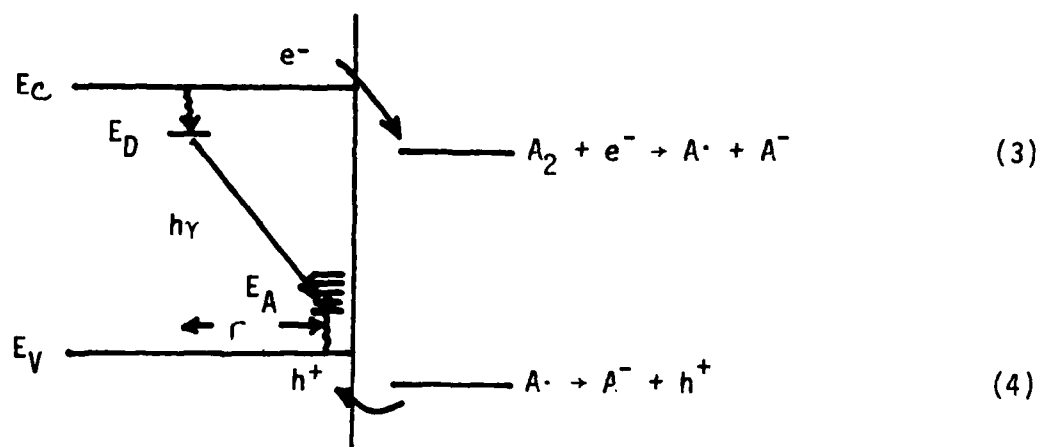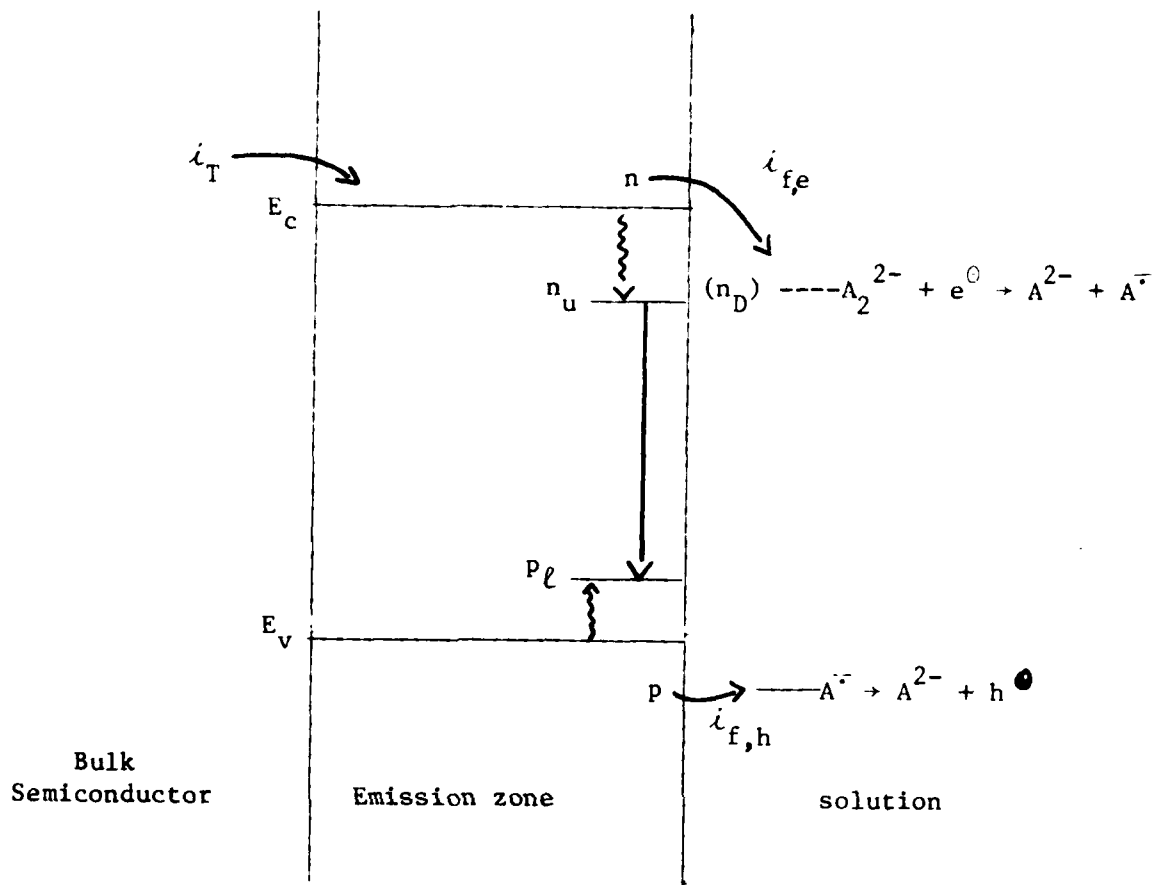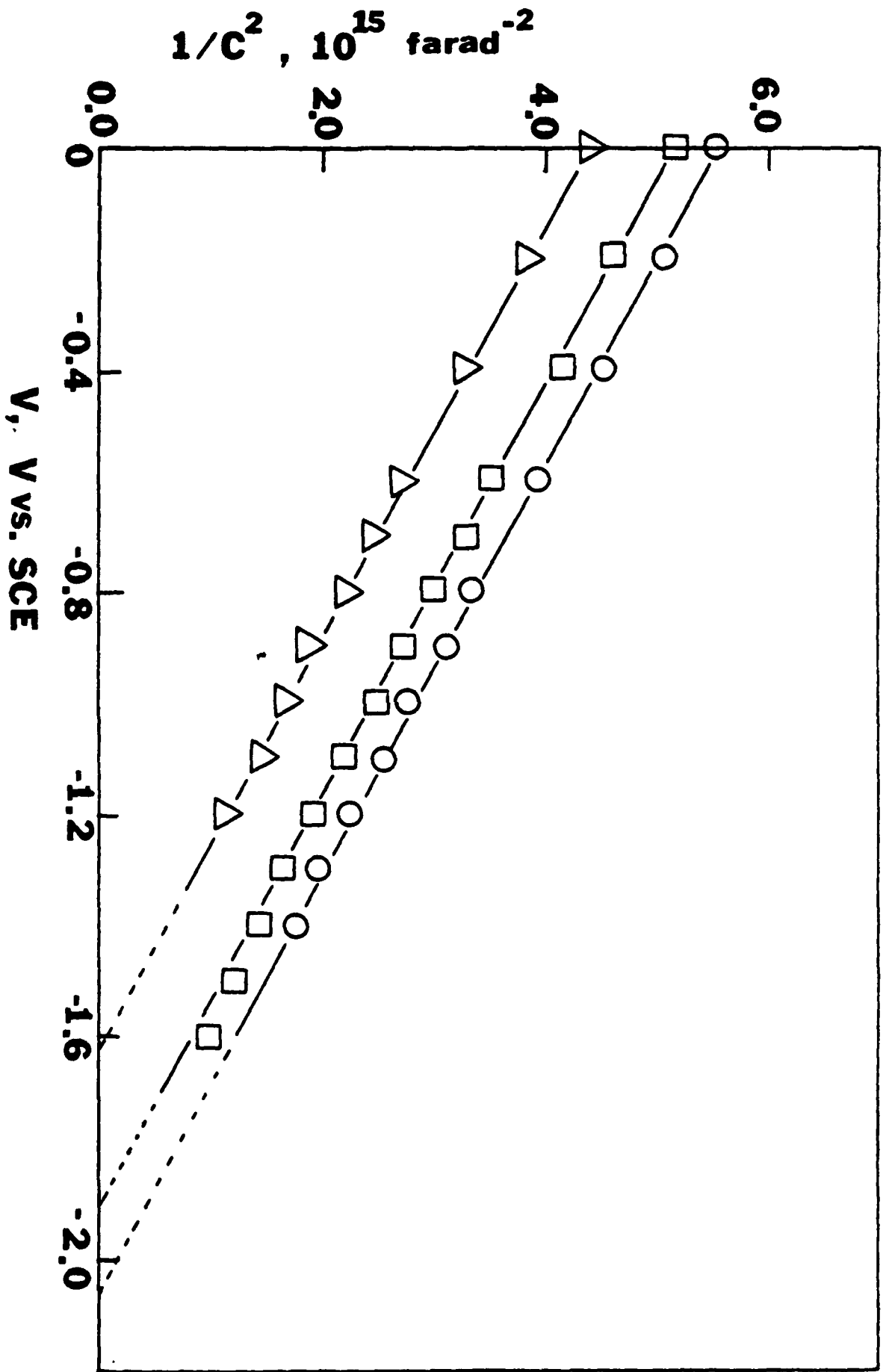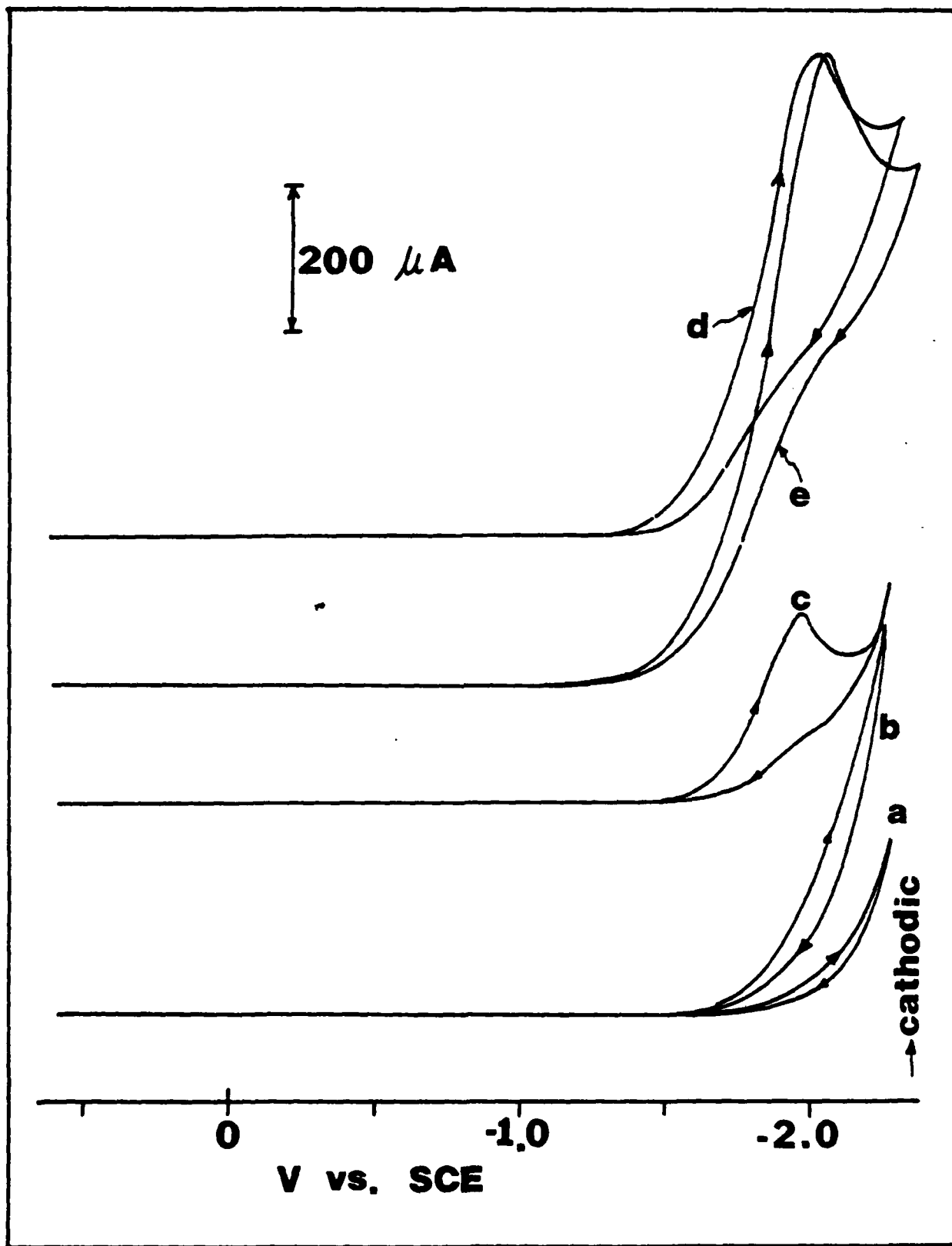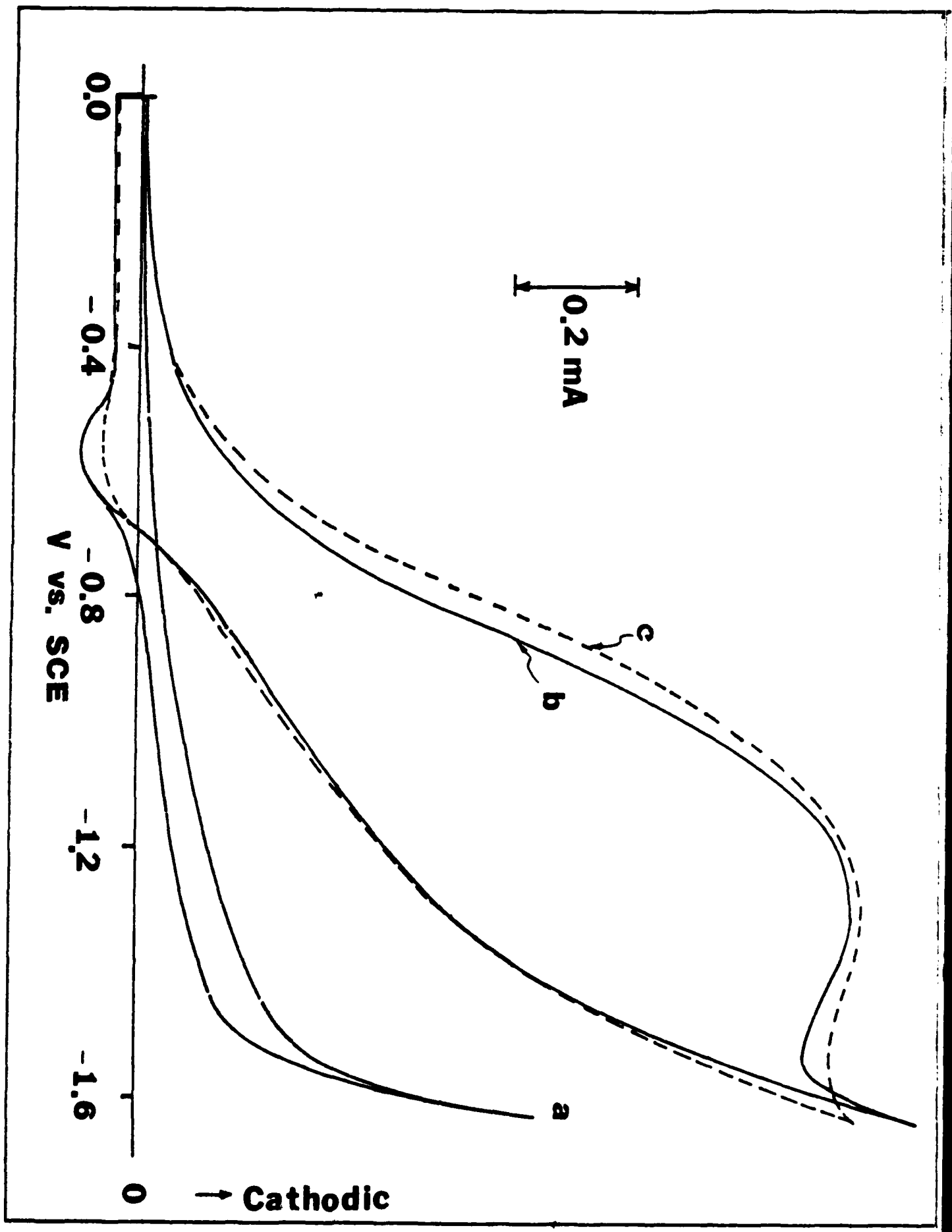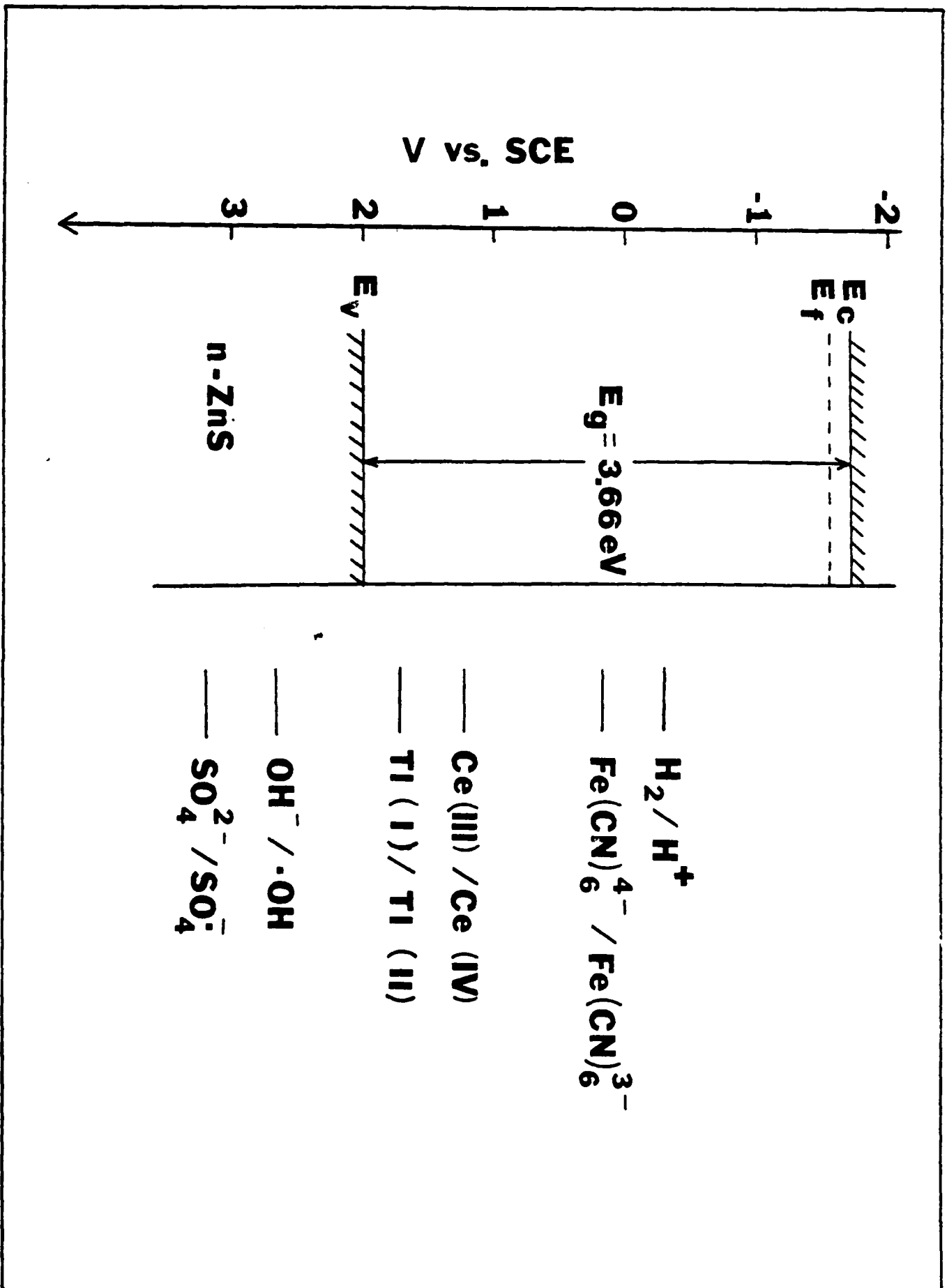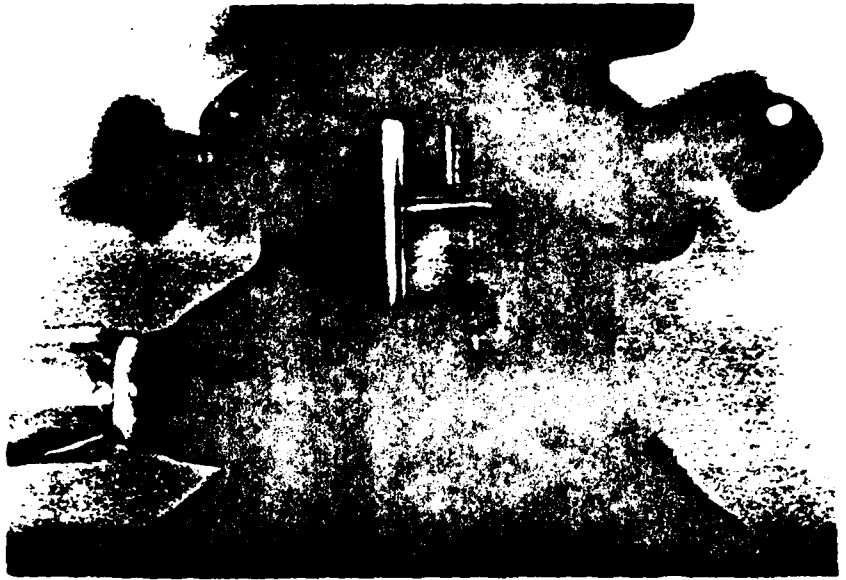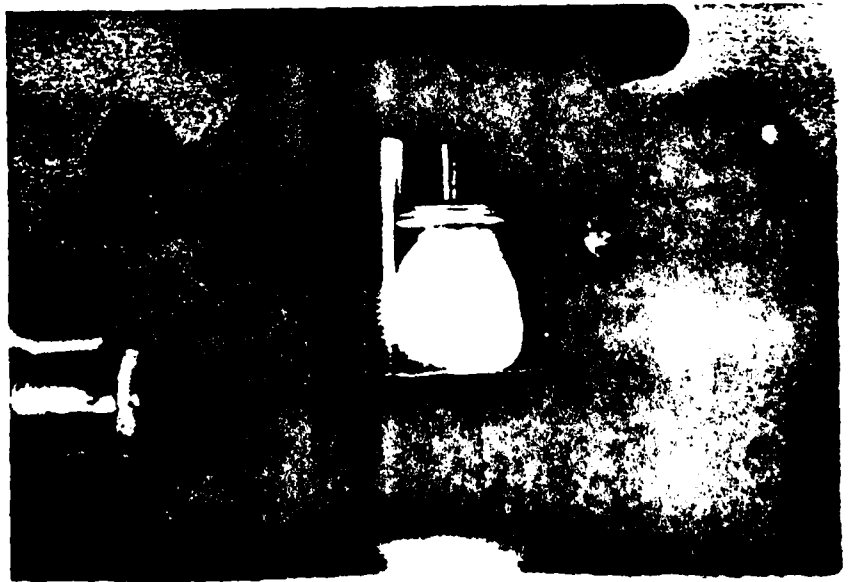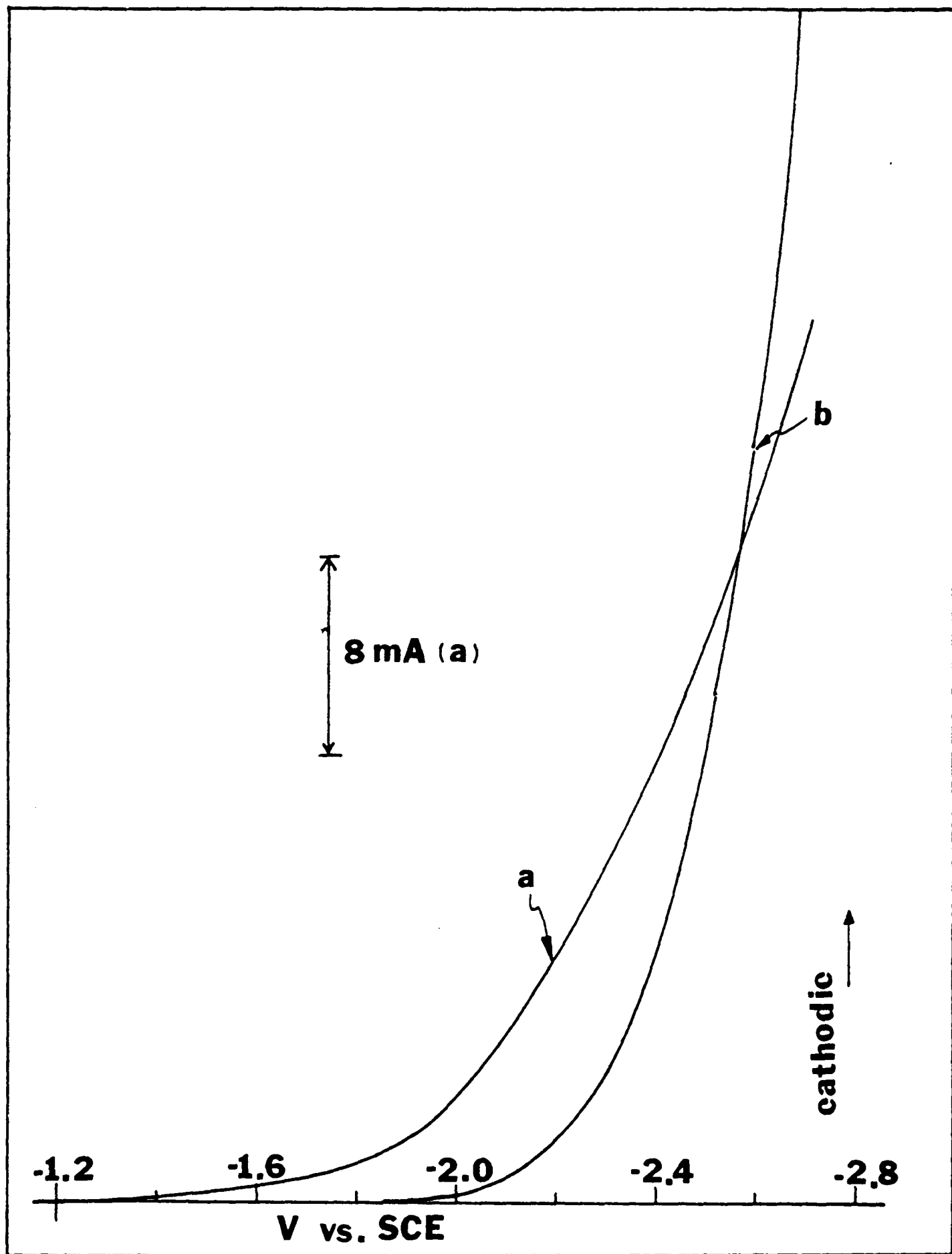
Fig. 6
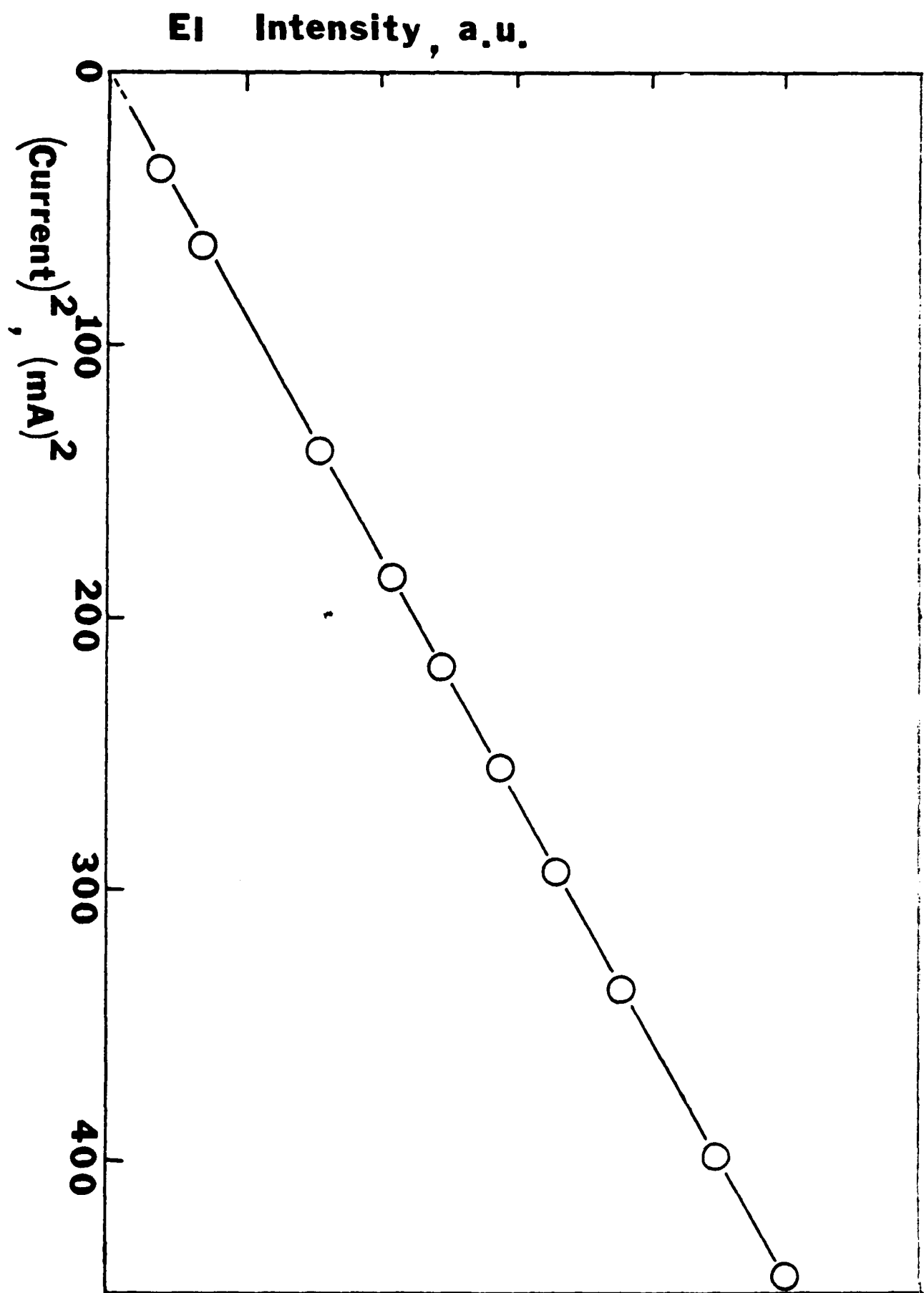
Fig.
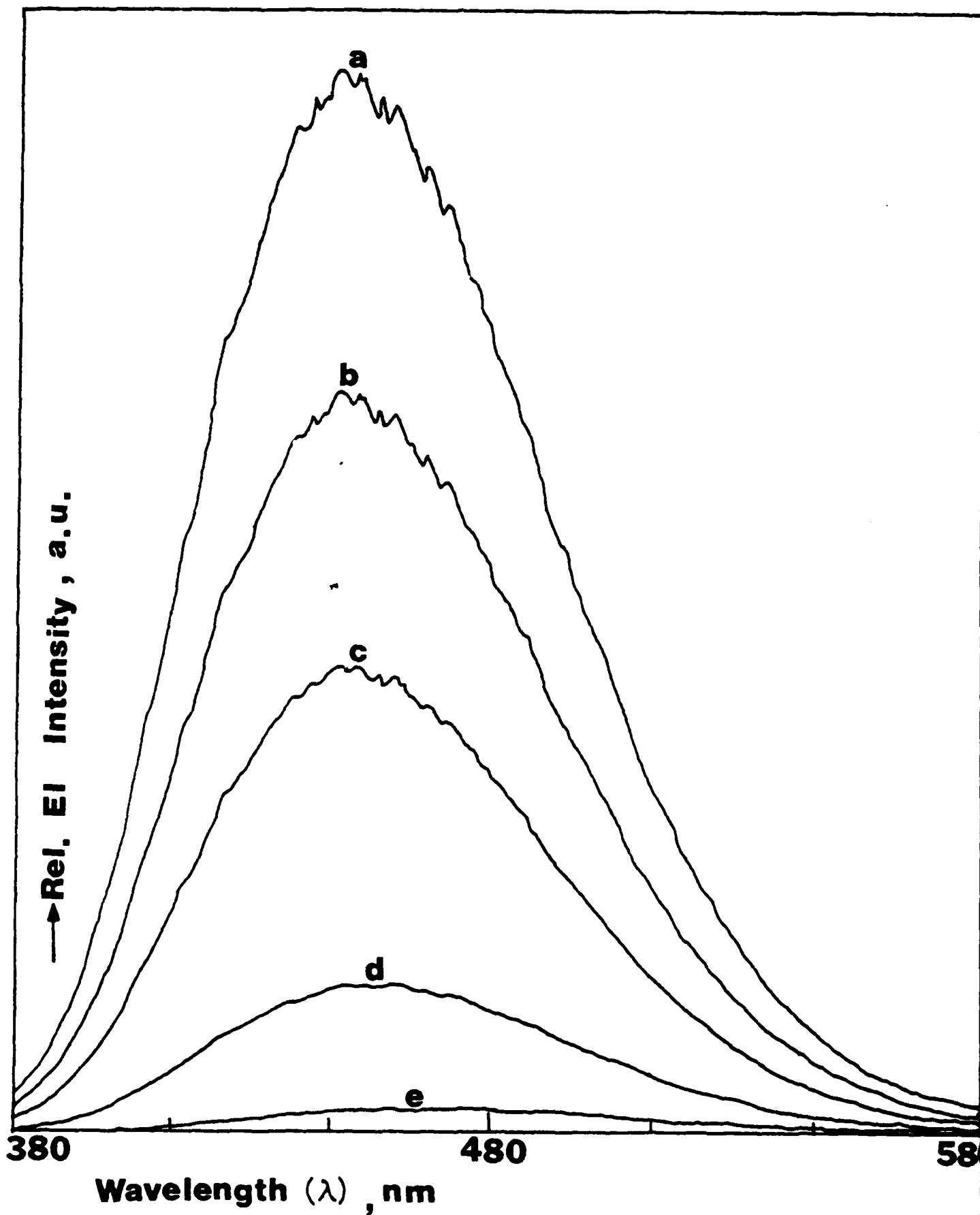
Fig.

Fig.

Fig.

Fig.

Fig. 12

Fig. 1

Axis labels:
- Y-axis: →Rel. EI Intensity, a.u.
- X-axis: Wavelength, nm

X-axis values: 380, 480, 580

Curve labels: a, b, c, d, e, f

El Intensity, a.u.

Time

1 ms

x4

x2

a

b

c

Fig. 1

$$A_2 + e^- \rightarrow A\cdot + A^- \qquad (3)$$

$$A\cdot \rightarrow A^- + h^+ \qquad (4)$$
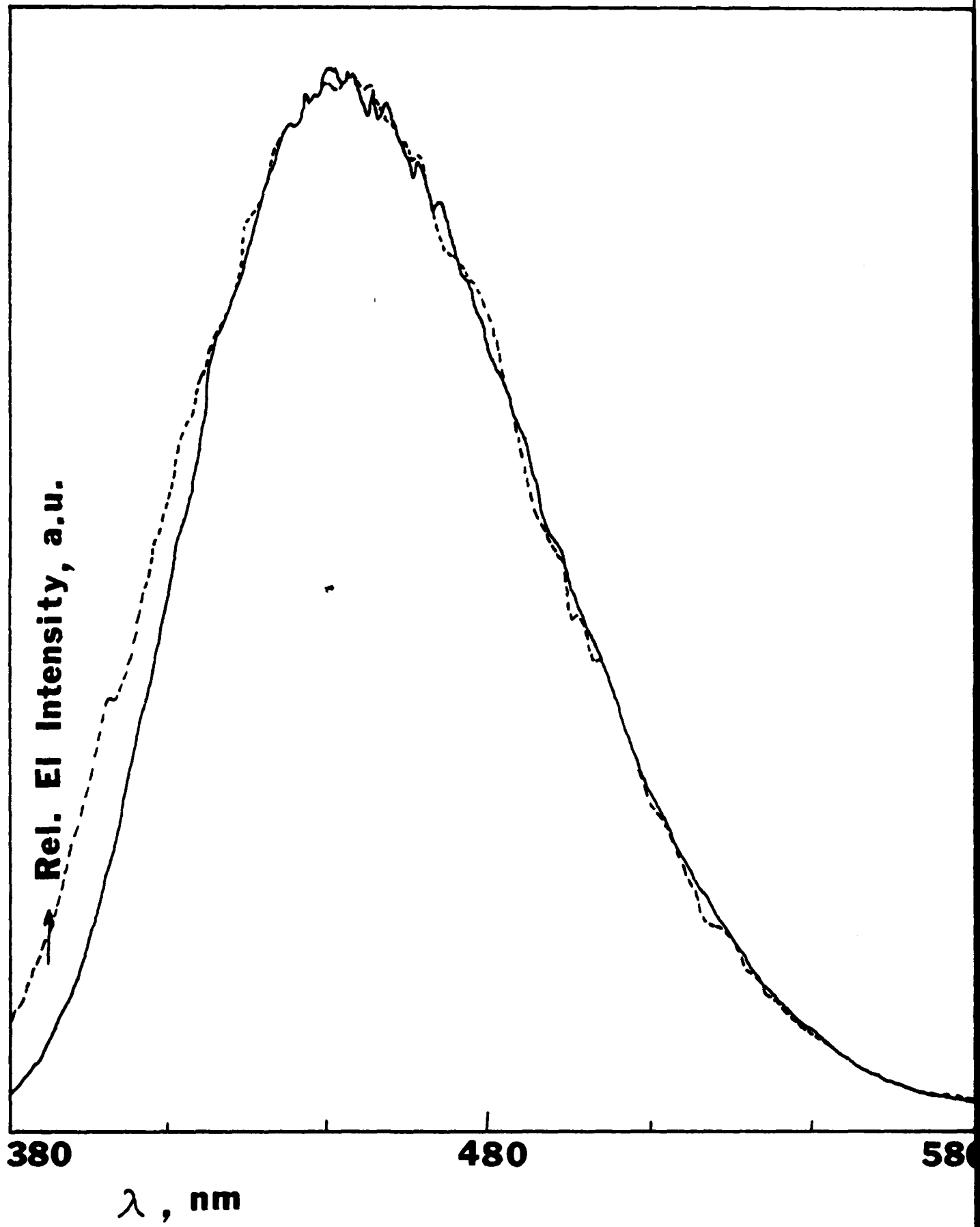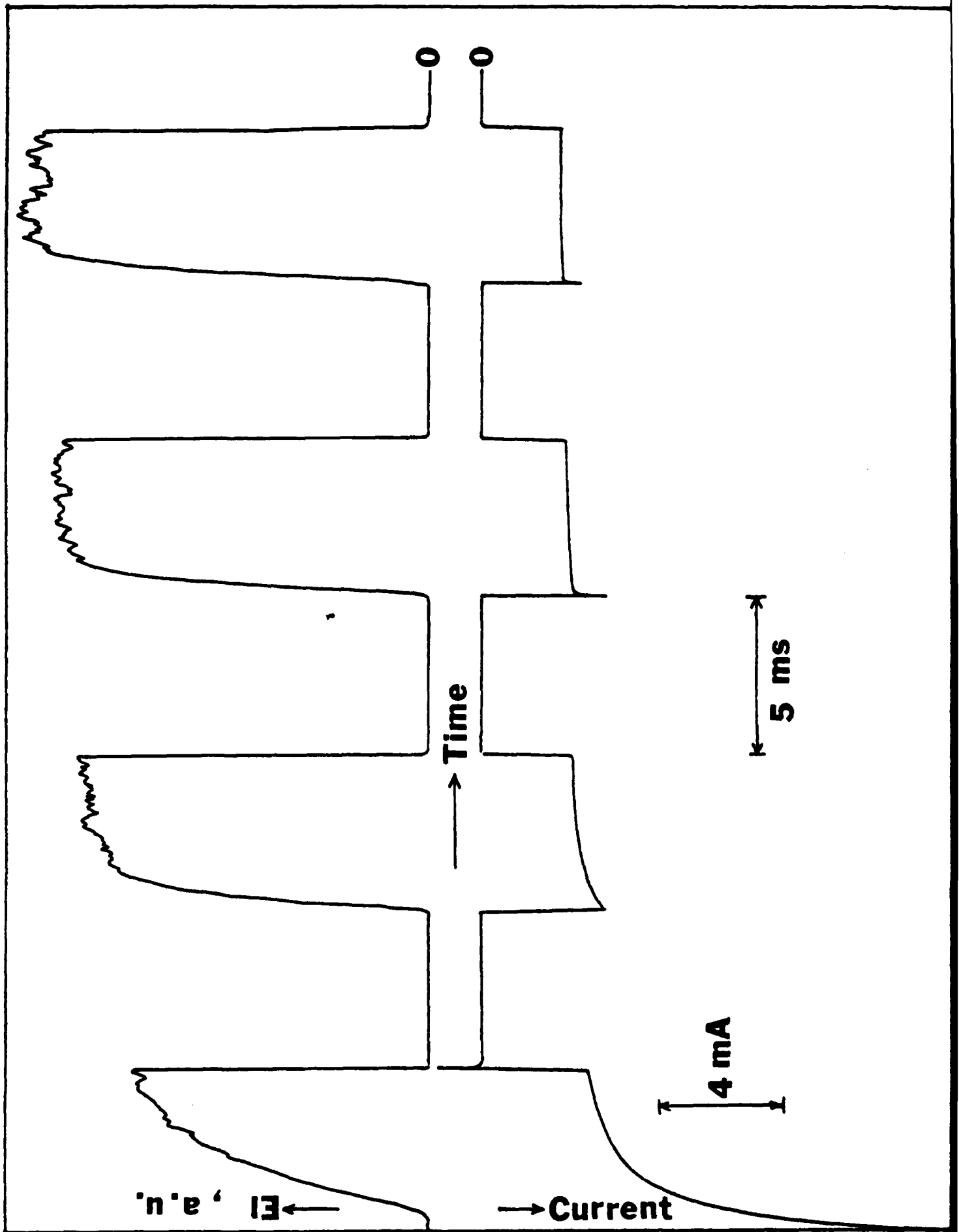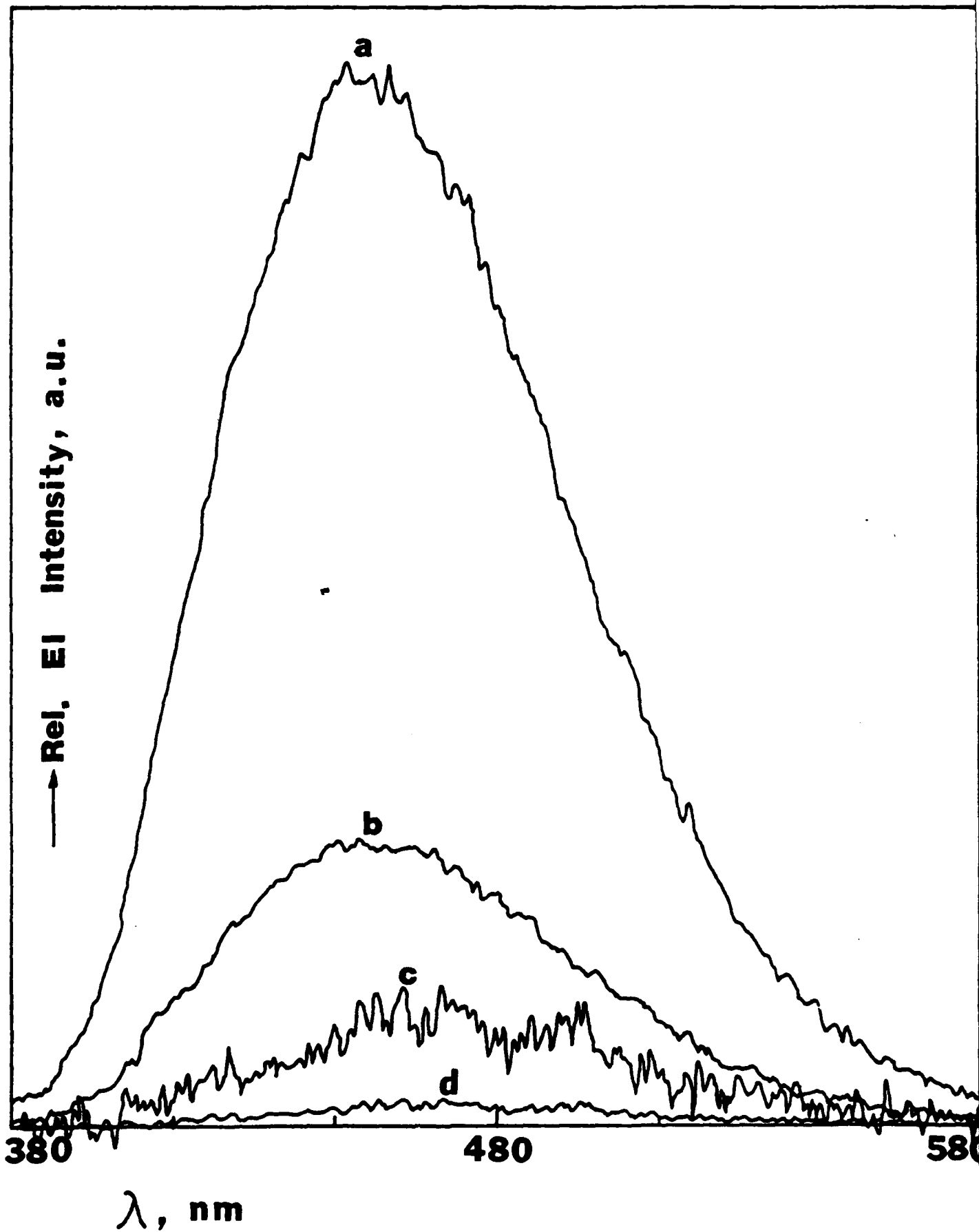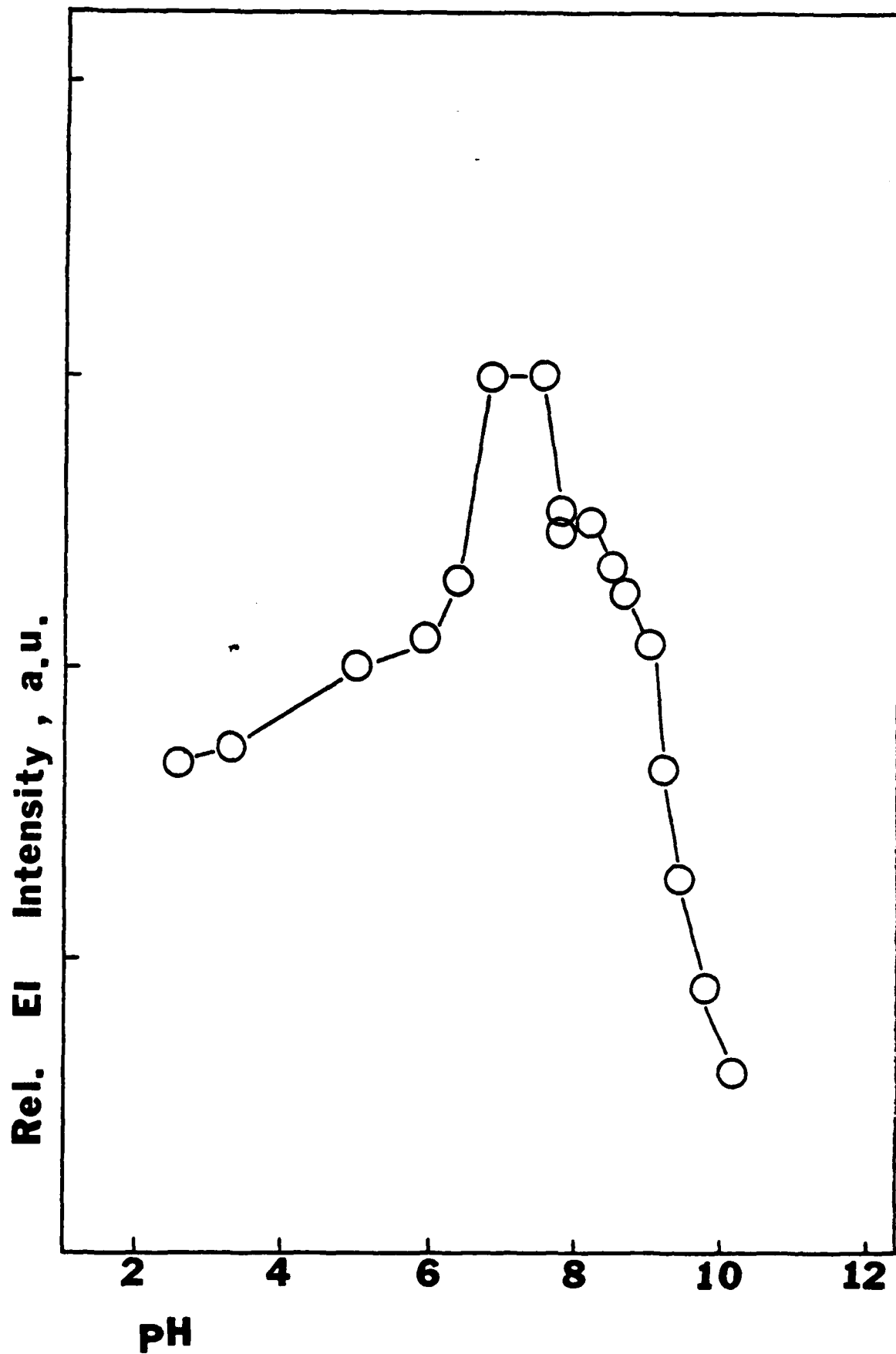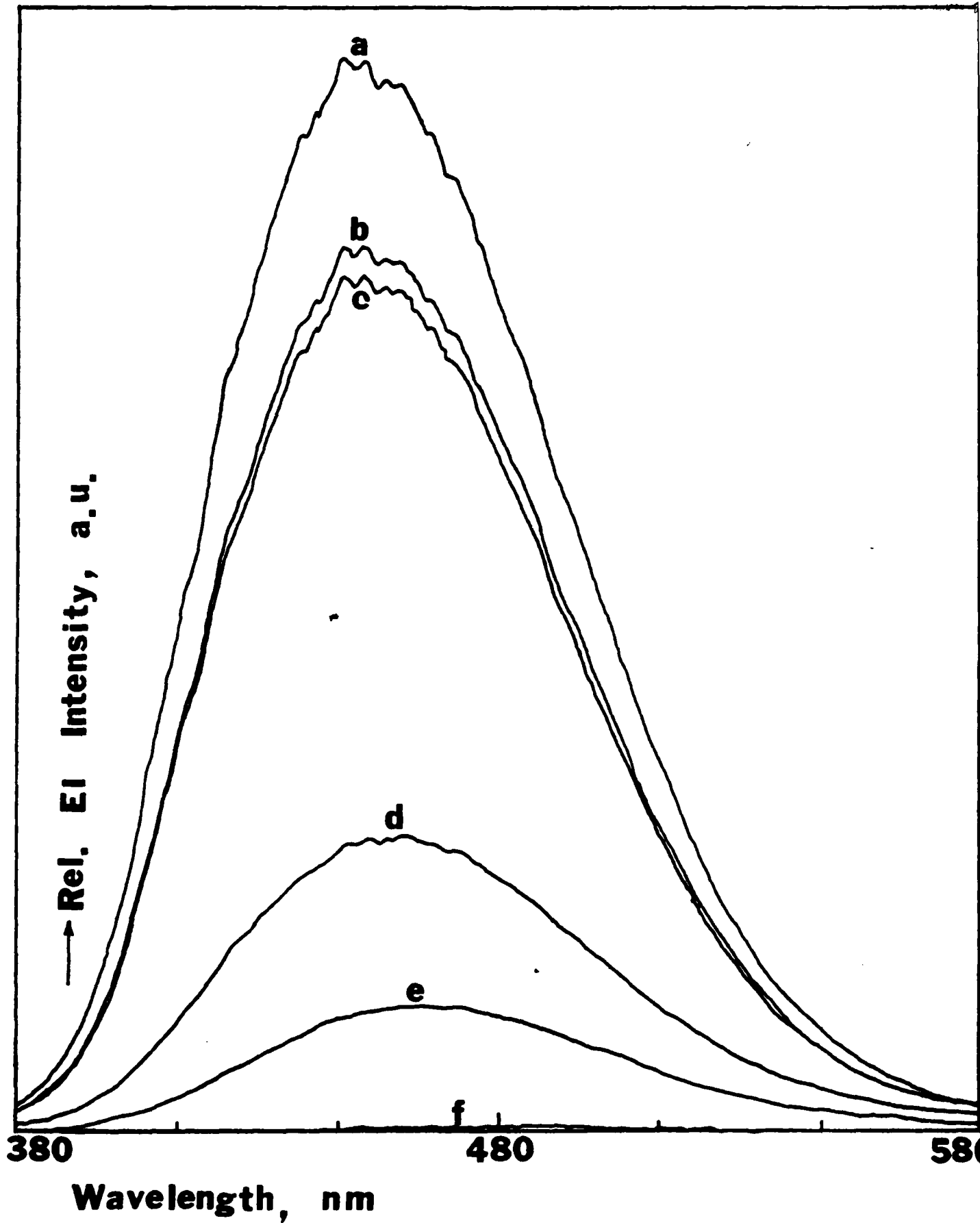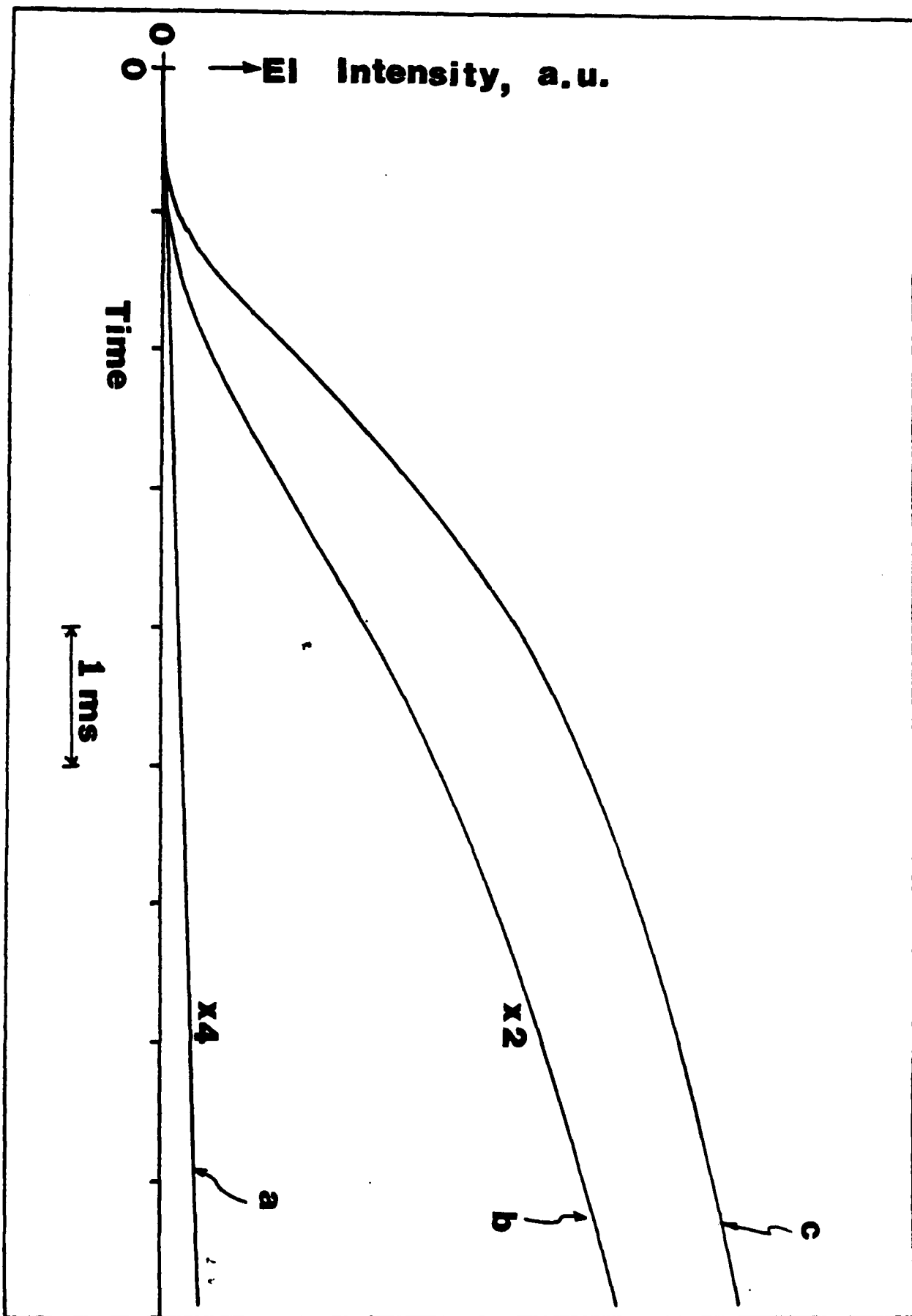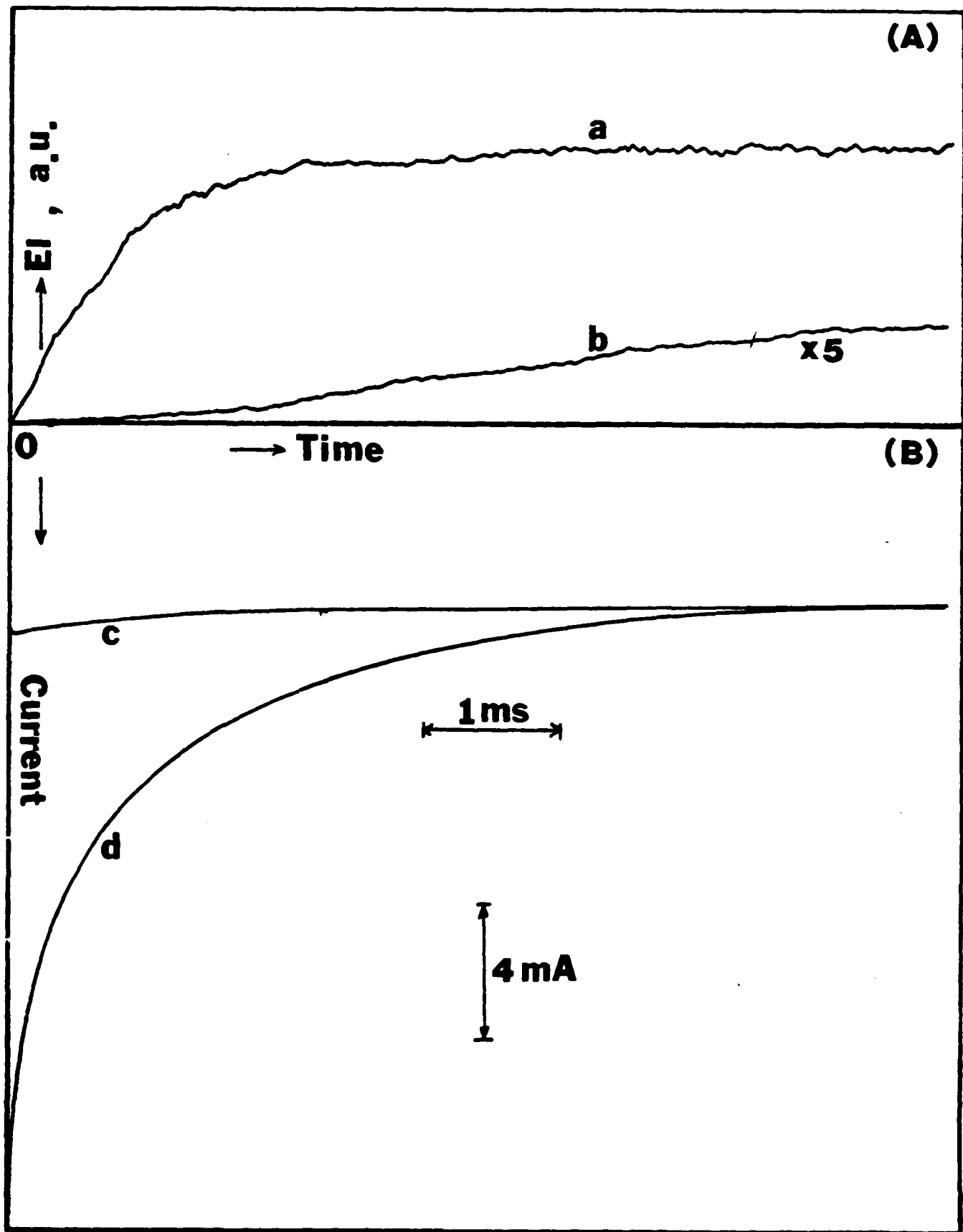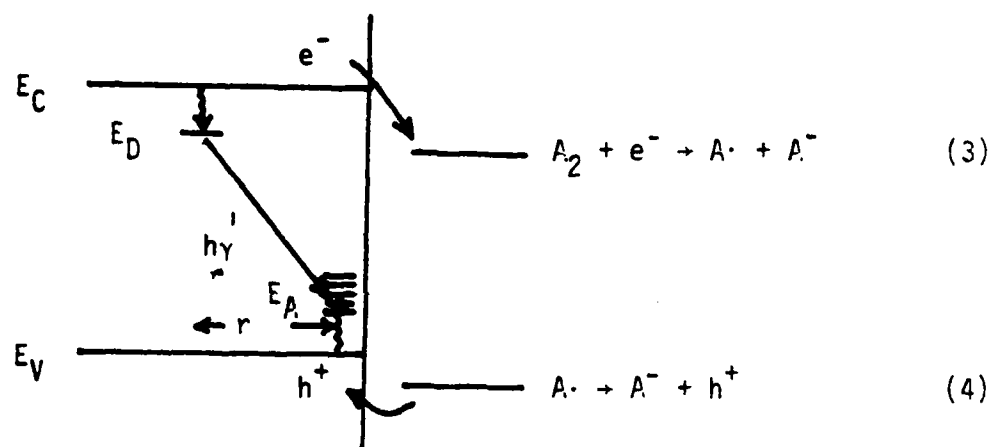
Scheme I

TECHNICAL REPORT DISTRIBUTION LIST, GEN

	No. Copies		No. Copies

Office of Naval Research
Attn: Code 413
800 North Quincy Street
Arlington, Virginia 22217 — 2

ONR Pasadena Detachment
Attn: Dr. R. J. Marcus
1030 East Green Street
Pasadena, California 91106 — 1

Commander, Naval Air Systems Command
Attn: Code 310C (H. Rosenwasser)
Department of the Navy
Washington, D.C. 20360 — 1

Defense Technical Information Center
Building 5, Cameron Station
Alexandria, Virginia 22314 — 12

Dr. Fred Saalfeld
Chemistry Division, Code 6100
Naval Research Laboratory
Washington, D.C. 20375 — 1

U.S. Army Research Office
Attn: CRD-AA-IP
P. O. Box 12211
Research Triangle Park, N.C. 27709 — 1

Mr. Vincent Schaper
DTNSRDC Code 2803
Annapolis, Maryland 21402 — 1

Naval Ocean Systems Center
Attn: Dr. S. Yamamoto
Marine Sciences Division
San Diego, California 91232 — 1

Naval Ocean Systems Center
Attn: Mr. Joe McCartney
San Diego, California 92152 — 1

Naval Weapons Center
Attn: Dr. A. B. Amster,
Chemistry Division
China Lake, California 93555 — 1

Naval Civil Engineering Laboratory
Attn: Dr. R. W. Drisko
Port Hueneme, California 93401 — 1

Dean William Tolles
Naval Postgraduate School
Monterey, California 93940 — 1

Scientific Advisor
Commandant of the Marine Corps
(Code RD-1)
Washington, D.C. 20380 — 1

Naval Ship Research and Development
Center
Attn: Dr. G. Bosmajian, Applied
Chemistry Division
Annapolis, Maryland 21401 — 1

Mr. John Boyle
Materials Branch
Naval Ship Engineering Center
Philadelphia, Pennsylvania 19112 — 1

Mr. A. M. Anzalone
Administrative Librarian
PLASTEC/ARRADCOM
Bldg 3401
Dover, New Jersey 07801 — 1

TECHNICAL REPORT DISTRIBUTION LIST, 359

	No. Copies		No. Copies

Dr. Paul Delahay
Department of Chemistry
New York University
New York, New York 10003 — 1

Dr. E. Yeager
Department of Chemistry
Case Western Reserve University
Cleveland, Ohio 41106 — 1

Dr. D. N. Bennion
Department of Chemical Engineering
Brigham Young University
Provo, Utah 84602 — 1

Dr. R. A. Marcus
Department of Chemistry
California Institute of Technology
Pasadena, California 91125 — 1

Dr. J. J. Auborn
Bell Laboratories
Murray Hill, New Jersey 07974 — 1

Dr. Adam Heller
Bell Laboratories
Murray Hill, New Jersey 07974 — 1

Dr. T. Katan
Lockheed Missiles and
Space Co., Inc.
P. O. Box 504
Sunnyvale, California 94088 — 1

Dr. Joseph Singer, Code 302-1
NASA-Lewis
21000 Brookpark Road
Cleveland, Ohio 44135 — 1

Dr. B. Brummer
EIC Incorporated
55 Chapel Street
Newton, Massachusetts 02158 — 1

Library
P. R. Mallory and Company, Inc.
Northwest Industrial Park
Burlington, Massachusetts 01803 — 1

Dr. P. J. Hendra
Department of Chemistry
University of Southampton
Southampton SOO 5NH
United Kingdom — 1

Dr. Sam Perone
Chemistry & Materials
Science Department
Laurence Livermore National Lab.
Livermore, California 94550 — 1

Dr. Royce W. Murray
Department of Chemistry
University of North Carolina
Chapel Hill, North Carolina 27514 — 1

Naval Ocean Systems Center
Attn: Technical Library
San Diego, California 92152 — 1

Dr. C. E. Mueller
The Electrochemistry Branch
Materials Division, Research and
Technology Department
Naval Surface Weapons Center
White Oak Laboratory
Silver Spring, Maryland 20910 — 1

Dr. G. Goodman
Johnson Controls
5757 North Green Bay Avenue
Milwaukee, Wisconsin 53201 — 1

Dr. J. Boechler
Electrochimica Corporation
Attn: Technical Library
2485 Charleston Road
Mountain View, California 94040 — 1

Dr. P. P. Schmidt
Department of Chemistry
Oakland University
Rochester, Michigan 48063 — 1

TECHNICAL REPORT DISTRIBUTION LIST, 359

No.
Copies

No.
Copi

Dr. H. Richtol Chemistry Department Rensselaer Polytechnic Institute Troy, New York 12181 1	Dr. R. P. Van Duyne Department of Chemistry Northwestern University Evanston, Illinois 60201 1
Dr. A. B. Ellis Chemistry Department University of Wisconsin Madison, Wisconsin 53706 1	Dr. B. Stanley Pons Department of Chemistry University of Alberta Edmonton, Alberta CANADA T6G 2G2 1
Dr. M. Wrighton Chemistry Department Massachusetts Institute of Technology Cambridge, Massachusetts 02139	Dr. Michael J. Weaver Department of Chemistry Michigan State University East Lansing, Michigan 48824 1
Larry E. Plew Naval Weapons Support Center Code 30736, Building 2906 Crane, Indiana 47522 1	Dr. R. David Rauh EIC Corporation 55 Chapel Street Newton, Massachusetts 02158 1
S. Ruby DOE (STOR) 600 E Street Providence, Rhode Island 02192 1	Dr. J. David Margerum Research Laboratories Division Hughes Aircraft Company 3011 Malibu Canyon Road Malibu, California 90265 1
Dr. Aaron Wold Brown University Department of Chemistry Providence, Rhode Island 02192 1	Dr. Martin Fleischmann Department of Chemistry University of Southampton Southampton 509 5NH England 1
Dr. R. C. Chudacek McGraw-Edison Company Edison Battery Division Post Office Box 28 Bloomfield, New Jersey 07003 1	Dr. Janet Osteryoung Department of Chemistry State University of New York at Buffalo Buffalo, New York 14214 1
Dr. A. J. Bard University of Texas Department of Chemistry Austin, Texas 78712 1	Dr. R. A. Osteryoung Department of Chemistry State University of New York at Buffalo Buffalo, New York 14214 1
Dr. M. M. Nicholson Electronics Research Center Rockwell International 3370 Miraloma Avenue Anaheim, California 1	

TECHNICAL REPORT DISTRIBUTION LIST, 359

No.
Copies

N
Cop

Dr. Donald W. Ernst
Naval Surface Weapons Center
Code R-33
White Oak Laboratory
Silver Spring, Maryland 20910   1

Mr. James R. Moden
Naval Underwater Systems
  Center
Code 3632
Newport, Rhode Island 02840   1

Dr. R. Nowak
Naval Research Laboratory
Code 6130
Washington, D.C. 20375   1

Dr. Bernard Spielvogel
U. S. Army Research Office
P. O. Box 12211
Research Triangle Park, NC 27709   1

Dr. John F. Houlihan
Shenango Valley Campus
Pennsylvania State University
Sharon, Pennsylvania 16146   1

Dr. Denton Elliott
Air Force Office of
  Scientific Research
Bolling AFB
Washington, D.C. 20332   1

Dr. D. F. Shriver
Department of Chemistry
Northwestern University
Evanston, Illinois 60201   1

Dr. David Aikens
Chemistry Department
Rensselaer Polytechnic Institute
Troy, New York 12181   1

Dr. D. H. Whitmore
Department of Materials Science
Northwestern University
Evanston, Illinois 60201   1

Dr. A. P. B. Lever
Chemistry Department
York University
Downsview, Ontario M3J1P3
Canada   1

Dr. Alan Bewick
Department of Chemistry
The University
Southampton, SO9 5NH England

Dr. Stanislaw Szpak
Naval Ocean Systems Center
Code 6343
San Diego, California 95152   1

Dr. A. Himy
NAVSEA-5433
NC #4
2541 Jefferson Davis Highway
Arlington, Virginia 20362

Dr. Gregory Farrington
Department of Materials Science
  and Engineering
University of Pennsylvania
Philadelphia, Pennsylvania 19104

Dr. John Kincaid
Department of the Navy
Strategic Systems Project Office
Room 901
Washington, D.C. 20376

Dr. Bruce Dunn
Department of Engineering &
  Applied Science
University of California
Los Angeles, California 90024

TECHNICAL REPORT DISTRIBUTION LIST, 359

	No. Copies		No Copi

M. L. Robertson
Manager, Electrochemical
  and Power Sonices Division
Naval Weapons Support Center
Crane, Indiana 47522   1

Dr. Elton Cairns
Energy & Environment Division
Lawrence Berkeley Laboratory
University of California
Berkeley, California 94720   1

Dr. Micha Tomkiewicz
Department of Physics
Brooklyn College
Brooklyn, New York 11210   1

Dr. Lesser Blum
Department of Physics
University of Puerto Rico
Rio Piedras, Puerto Rico 00931   1

Dr. Joseph Gordon, II
IBM Corporation
K33/281
5600 Cottle Road
San Jose, California 95193   1

Dr. Robert Somoano
Jet Propulsion Laboratory
California Institute of Technology
Pasadena, California 91103   1

Dr. Johann A. Joebstl
USA Mobility Equipment R&D Command
DRDME-EC
Fort Belvior, Virginia 22060   1

Dr. Judith H. Ambrus
NASA Headquarters
M.S. RTS-6
Washington, D.C. 20546   1

Dr. Albert R. Landgrebe
U.S. Department of Energy
M.S. 6B025 Forrestal Building
Washington, D.C. 20595   1

Dr. T. Marks
Department of Chemistry
Northwestern University
Evanston, Illinois 60201   1

Dr. D. Cipris
Allied Corporation
P. O. Box 3000R
Morristown, New Jersey 07960   1

Dr. M. Philpot
IBM Corporation
5600 Cottle Road
San Jose, California 95193   1

Dr. Donald Sandstrom
Washington State University
Department of Physics
Pullman, Washington 99164   1

Dr. Carl Kannewurf
Northwestern University
Department of Electrical Engineering
  and Computer Science
Evanston, Illinois 60201   1

Dr. Edward Fletcher
University of Minnesota
Department of Mechanical Engineering
Minneapolis, Minnesota 55455   1

Dr. John Fontanella
U.S. Naval Academy
Department of Physics
Annapolis, Maryland 21402   1

Dr. Martha Greenblatt
Rutgers University
Department of Chemistry
New Brunswick, New Jersey 08903   1

Dr. John Wassib
Kings Mountain Specialties
P. O. Box 1173
Kings Mountain, North Carolina 28086   1

TECHNICAL REPORT DISTRIBUTION LIST, 359

	No. Copies		No. Copies

Dr. J. J. Brophy
University of Utah
Department of Physics
Salt Lake City, Utah 84112   1

Dr. Walter Roth
Department of Physics
State University of New York
Albany, New York 12222   1

Dr. Thomas Davis
National Bureau of Standards
Polymer Science and
  Standards Division
Washington, D.C. 20234   1

Dr. Charles Martin
Department of Chemistry
Texas A&M University   1

Dr. Anthony Sammells
Institute of Gas Technology
3424 South State Street
Chicago, Illinois 60616   1

Dr. H. Tachikawa
Department of Chemistry
Jackson State University
Jackson, Mississippi 39217   1

Dr. W. M. Risen
Department of Chemistry
Brown University
Providence, Rhode Island   1

END

FILMED

5-83

DTIC